Thermonavigation of Convective Plumes in the Mosquito *Aedes aegypti*

Sharri A. Zamore

A dissertation submitted in partial fulfillment of the requirements for the degree of

Doctor of Philosophy

University of Washington

2015

Reading Committee:

Adrienne Fairhall, Chair

Tom Daniel

Jeff Riffell

Program Authorized to Offer Degree:

Neurobiology and Behavior

Abstract

The yellow fever mosquito, *Aedes aegypti*, is a vector for numerous diseases, including Dengue fever, Chikungunya, and yellow fever. Efforts to minimize transmission of this disease focus on minimizing vector-host interactions, with a centralized effort to elucidate strategies employed to effectively locate hosts via windborne cues. Efforts to understand how host-emitted plumes are navigated focus on olfaction. While olfaction allows for easily controlled stimuli and robust behavioral response, it is not the only sensory modality employed during host localization. Indeed, deterrents that inhibit olfactory detection do not fully inhibit host localization. Mosquitoes are well endowed with many sensory receptors for several sensory modalities, including thermosensation.

I present a series of experiments that examine and describe plume navigation in response to convective thermal plumes. Female mosquitoes were flown in a wind tunnel (1 m long x 0.26 m wide x 0.26 m tall) with a constant wind speed of 0.5 ± 0.05 m s-1, and either no thermal signal, or a lateralized (left or right) thermal plume present. The heating elements of these plumes were modified such that radiative signal was minimized, resulting in stimulus comprised of only convective thermal signal at distances where behaviors were measured. These thermal plumes were turbulent in structure, and produced temperature differences of up to 6 °C. We defined the location and boundaries of these plumes using a mathematical model based on temperature differences, flow speed, and rates at which the plume mixed in external air.

I show, for the first time, that mosquitoes navigate toward thermal sources using only convective signals. The plume navigation behavior is described by a bias to the crosswind (lateral) position of the plume source ($p < 0.01$), and is achieved by augmenting the ratio of left and right turns during flight. A trend of slowly shifting, or sometimes oscillating, the average heading of the trajectory was also found, and may suggest another thermonavigation strategy.

Large scale effects such as these were seen, however no change in distributions or features of kinematics (e.g. velocity, acceleration) were seen. To determine whether such slight changes or biases in kinematics can produce these large scale behaviors by creating an agent based model of mosquito flight. Features of mosquito navigation were approximated by modeling flight as a biased random walk in a driven damped mass system. The model was trained on control (plume absent) behavior, and tested with the presence of the plume, which was represented as a binary signal at the position of the empirical plumes. We defined a stimulus bias as a slight bias toward the last crosswind position a plume was detected, and faster upwind velocities while within the plume bounds. The agent model did not produce the control crosswind distributions, but did produce crosswind position distributions similar to those observed in mosquito behavior, and had similar kinematics in and outside of the plume boundaries.

These experiments demonstrate that mosquitoes, when presented a turbulent, convective thermal plume, navigate in a biased random walk, and augment the bias of the walk toward the crosswind plume location.

I dedicate this dissertation to my father, for nurturing my interest in the natural world, my grandmother, for supporting me through college and beyond, and Nicki Minaj for always encouraging women to seek and prioritize education. This work is also dedicated to my mother, for teaching me the fortitude and resilience required for success.

Acknowledgements

The collection of work presented here is the work of many minds coming together, offering wisdom, encouragement, knowledge, criticism, and selflessness. I extend the deepest of gratitude to my two advisors, Drs. Adrienne Fairhall and Tom Daniel for their patience, foresight, and remarkable intellect. It has truly been a pleasure working with and learning from brilliance such as theirs. This gratitude is also extended to the remaining members of my committee, Dr. Jeff Riffell, Dr. Nathan Kutz and Dr. Michael Dickinson. The behavioral setup and paradigm was focused largely by the efforts of Dr. Michael Dickinson and generosity of his lab members, especially Floris van Breugel, Steve Safarik, and Johan Melis. I am especially grateful for the perspective, rigor and support of Dr. Jeff Riffell throughout the entire duration of this project.

Many thanks to Dr. Mark Willis and Dr. Bob Breidenthaal for help developing the thermal plume model, for fostering a genuine curiosity about mosquitoes and the environments encounter.

This project would not have come to fruition without the tireless work, skill, and excellence of Valentina Staneva, Ricardo Decal and Richard Pang. I deeply appreciate your outstanding intellect and impressive work ethic.

I am grateful for the support, knowledge and encouragement from my labmates, collaborators, and peers, especially Mike Famulare, Heather Barnett, Allison Duffy, Armin Hinterwirth, Annika Eberle, Bing Brunton, Yonoton Munk, and Brad Dickerson. You all are the best labmates one could chance to have.

Finally, I extend humble gratitude to the National Institutes of Health (Neurobiology and Behavior Training Grant), the Endowed Komen Chair, and Nature Inspired Flight Technology and Ideas, for providing financial support for this research.

Table of Contents

List of Figures **3**

I. Introduction **4**

1. The Navigation Problem *4*

2. Mosquito Sensilla: Morphology and Response *5*

3. Spatiotemporal Features of Windborne Stimuli *7*

4. Plume Navigation in Mosquitoes *10*

5. Proposed Experiments *11*

References *12*

II. Experimental Design and Plume Modeling **14**

Abstract *14*

Introduction *14*

Materials and Methods *18*

Results *22*

Discussion *27*

References *31*

III. Behavioral Evidence of Convective Plume Tracking during Flight in The Mosquito (*Aedes aegypti*) **33**

Abstract *33*

Introduction *33*

Methods *35*

Results *42*

Discussion *47*

References *51*

IV. Modeling Behavioral Policy of Thermonavigation **53**

Abstract *53*
Introduction *53*
Methods and Materials *57*
Results *61*
Discussion *66*
References *69*

V. Concluding Remarks 71

List of Figures

Chapter I.

1.1 - Location and features of thermosensilla in *Ae. aegypti*.

1.2 - Spatiotemporal features of flow regimes.

Chapter II.

2.1 - Schematic of predicted thermal plume in crossflow.

2.2 - Time averaged and spatial probability distribution of wind tunnel temperatures.

2.3 -Vertical rise and radius of the plume as a function of distance.

2.4 - Measurements of plume densities and dilution rates.

2.5 - Theoretically derived plume boundaries.

Chapter III.

3.1 - Experimental setup and measurements.

3.2 - Distributions of trajectory positions.

3.3 - Observed kinematics of flight.

3.4 - Kinematics in and out of plume boundaries.

3.5 - Heading angle distributions throughout wind tunnel volume.

Chapter IV.

4.1 - Examples of model and mosquito trajectories.

4.2 - Spatial density of positions.

4.3 - Position distributions of model.

4.4 - Model performance in comparison to behavior.

4.5 - Model kinematics.

I.

Introduction

Mosquitoes are vectors for several important human and animal diseases, including malaria, Dengue fever, yellow fever, Chikungunya, and heartworm. Malaria, for example, claims the lives of millions people per year, most of whom live in regions of the world that contain large percentages of the global population, such as India, China, Indonesia, Brazil, throughout the Caribbean, and the majority of countries throughout central and southern Africa (Hay et al., 2004). In all cases, mosquitoes must localize their hosts in complex environments using a variety of sensory cues. Thus, knowledge of mosquito host seeking behavior is crucial to the eradication of transmission of such mosquito-borne diseases. Thus, much mosquito behavioral research examines what and how mosquitoes detect various cues required to navigate to humans (Gibson & Carde, 2010). The present-known host localization behavior has been applied to the development of mosquito traps and deterrents.

With more explicit the knowledge of mosquito seeking behaviors, more effective and, importantly, affordable or accessible traps can be made and distributed in regions rife with mosquito-borne diseases. Presently, most effective mosquito traps use carbon dioxide to attract mosquitoes (Gibson and Cardé, 2010). Unfortunately, these traps are not available in regions plagued by mosquito-borne diseases due to high cost, and difficulty of access to CO_2 gas cylinders, dry ice or propane required for such traps. Understanding how mosquitoes use thermal signals to navigate toward humans could lend vital information in formulating efficient, affordable traps for regions affected by mosquito-borne disease. Such development of knowledge and technology is made urgent by ongoing climate change

To best study the interaction between humans and host-seeking mosquitoes, one should consider the problem from the mosquito's perspective. What role do thermal signals play in an individual's ability to localize a host?

1. The Navigation Problem

The female mosquito requires blood proteins to produce eggs. To achieve this goal, the hematophagous female flies through the environment to find her host-prey, changing her flight path with detection of host-emitted cues. There is a large suite of cues mosquitoes are able to detect, but the propagation of those cues through the environment makes this navigation task difficult. Locating host-prey requires detectable levels of cues, the persistence of cues throughout the environment, the ability to behaviorally respond to detection in a timely fashion, and behavioral decisions that improve the probability of detecting a cue. The difficulty of this task is further increased by the movement of the host-

prey, which augments the downwind distribution of navigatory cues, and active avoidance of the mosquito, which often happens in the case of human host-prey. Despite the difficulties, mosquitoes are able to detect and navigate toward humans from distances greater than 10 m, and can navigate to a source from that distance on the order of seconds (Bowen, 1991, Gibson and Cardé, 2010).

2. Mosquito Sensilla: Morphology and Response

Mosquitoes are equipped with a multitude of sensors, which can detect small and rapid changes in their environment. Many of the sensors are found on the antennae and maxillary palps (Figure 1.1A), including mechanosensors, olfactory sensors, and thermosensors. Female mosquitoes exhibit search behaviors, such as initiation of flight, directed flight toward the source, and landing, in response to local changes in humidity, skin and other odors, CO_2, and heat (Gibson and Cardé, 2010).

Carbon Dioxide Detection

Much host-seeking behavioral research and mosquito deterrents focus on olfaction as the primary modality. Mosquitoes have specific olfactory receptors that can bind odor particles of human sweat, carbon dioxide (CO_2), and lactic acid.

Sensilla on the maxillary palp drive responses to environmental CO_2 in a number of mosquito species, including *Aedes aegypti*. Electrophysiological recordings of the neural efferent show, with a 2 s presentation of CO_2, the spike rate first has a phasic increase, then decreases to some tonic firing pattern (Grant et al., 1995). It is suggested that the tonic firing rate of the CO_2-sensitive neurons encodes the background concentrations of carbon dioxide, while the phasic increase in firing rate encodes the change in concentration (Altner and Loftus, 1985, Majeed et al., 2013). The neurons can reliably respond to small changes (50 ppm) in concentration (Grant et al., 1995). The neural response is also known to vary with timing of the stimulus, at a resolution that allows the detection of changes in concentration that are typical to those seen in human-borne signals (Grant and O'Connell, 2007).

The length of the CO_2 presentation has electrophysiological and behavioral saliency. When *Ae. aegypti* is exposed to short presentations of CO_2 (< 2 s), there is a phasic CO_2 neural response. The firing rate after 2 s presentation of CO_2 adapts, but does not return to baseline, suggesting that the tonic firing rate encodes the "background" CO_2 concentration (Altner and Loftus, 1985). Behaviorally, short pulses of CO_2 increase behavioral response to other windborne chemical stimuli (Dekker et al., 2005).

When the CO_2 presentations are extended (> 2 s), neural adaptation takes place, ending the phasic response CO_2 (Turner et al., 2011). This phenomenon may allow mosquitoes to better navigate to sources, particularly when the signal is sparse, as often occurs with CO_2. Behavioral changes are seen when prolonged (> 1 min) chemical activation of the CO_2 receptor occurs, however, electrophysiological

studies have not been carried out. This prolonged stimulation renders mosquitoes unable to navigate to the source of olfactory stimuli, including CO_2 (Turner et al., 2011). Thus, the temporal fluctuation of CO_2 is requisite for mosquitoes to localize host prey via CO_2 stimuli.

Thermal Detection

Aedes aegypti possess a pair of thermosenilla at the distal end of each antenna (Figure 1.1B and 1.1C), each containing a singular thermoresponsive neuron. A neuron of one sensillum increases firing rate in response to an increase in temperature (warm cell), while the other decreases firing rate in response to an increase in temperature (cold cell) (Gingl et al., 2005). The firing rate of these neurons changes with instantaneous temperature and its rate of change.

Gingl et al. (2005) compared cellular response to radiative and convective thermal signals and found that, with convective stimuli, the thermoresponsive neurons' firing rates change with the rate and sign of temperature change. Presentation of radiative stimuli showed a change in response to absolute temperature, but rate or sign of change was not encoded. The authors show that neural adaptation seen in warm and cold cells encode rates of changes of temperature, and that these cells can encode small changes in temperature, as small as 0.002 °C s^{-1} (Tichy et al., 2008). The temporal acuity of thermosensation is unknown, so one cannot posit whether these responses are sufficient to detect temperature changes typically seen in their environments. It is also unclear whether mosquitoes are differentially sensitive to different types of thermal energy.

The structure of the sensillum suggests that mosquitoes are sensitive to convective thermal energy, perhaps more so than radiative energy. Most thermonavigating insects, such as the fire beetles (*Melanophila sp.*) and leaf-cutting ant (*Atta vollendweirdi*), possess sensilla with evolutionarily conserved structure, typically referred to as sensilla coeloconica, or peg-in-pit. These structures are comprised of a bowl-shaped cavity, with a protrusion extending from the floor of the bowl into the space of the cavity (McIver, 1973). A neuron extends into the peg, which responds to changes in temperature. In the mosquito, *Aedes aegypti*, the peg is notably sunken (Figure 1.1B), leaving only the tip available to absorb radiative energy. Because of these structural features, Gingl et al. (2005) suggest that the sensilla of *Aedes aegypti* are better suited to detect convective signals.

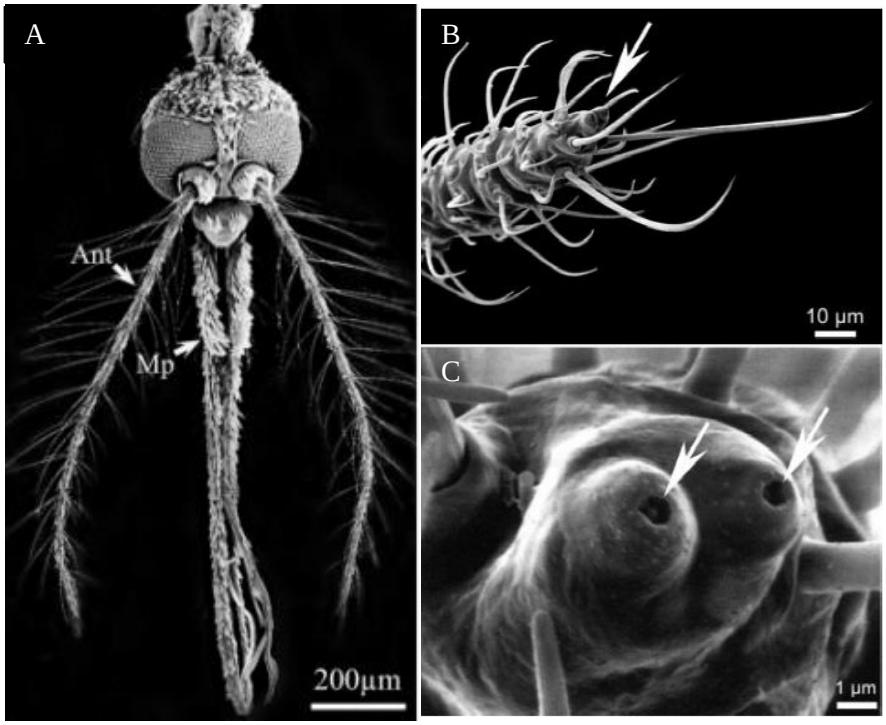

Figure 1.1 - Location and features of thermosensilla in *Ae. aegypti*. **A**) Location of antennae (Ant) and maxillary palps (Mp) on the head of *Aedes aegypti*. From Ghaninia et al., 2005, *Eur J Neurophysiol*. **B**) Coeloconic (peg-in-pit) sensors are found at the distal-most end of the antenna. **C**) Peg-in-pit structures have wall extending past the peg, limiting the available area. From Gingl et al., 2005, *J Neurophysiol*.

Mosquitoes behaviorally respond to changes in temperature, and likely can detect these changes via TRPA1 receptors, found in the peg-and-pit sensilla and throughout the antennae of *Anopheles gambiae* (Peterson and Brown, 1951, Bowen, 1991, Wang et al., 2009). The removal of antennae decreases the number of occurrences of landing on a warm plate in the mosquito *Anopheles stephensi*, suggesting that mosquitoes require intact thermosensilla to navigate toward a warm source (Maekawa et al., 2011).

3. Spatiotemporal Features of Windborne Stimuli

While the molecular, neural, morphological, and behavioral evidence all point to a crucial role of antennal thermosensors in host localization, several key issues remain unresolved. In particular, thermal energy is transported by a variety of mechanisms including radiative, conductive and convective transport (see for example, Campbell, 1977). Conductive energy exchange is not likely to be important, but both radiative and convective exchanges could theoretically each independently evoke receptor responses. Yet in natural environments, each have vastly different spatial temporal features. Moreover, the dynamics of convective transport heat exchange is further complicated by turbulent structures as well as thermally

induced buoyant forces. Thus, the temporal dynamics of the relevant thermal stimulus driving mosquito host seeking behavior remains an open problem. As such, we need to develop an understanding of the basic physics of energy and mass transport that are relevant to host-seeking behaviors.

A potential host is a source of thermal energy and, as mentioned above, some of that energy is transported by radiative exchange. In that case, the thermal signal appears more like a visual signal with the strength proportional to the host temperature (to the fourth power) and declines as the square of the distance from the source, though atmospheric attenuation (Bouguer's Law) contributes to a steeper decline. From the point of view of a mosquito, the detector of radiative heat would necessarily need to face the source, just like a photoreceptor.

In addition to energy loss by radiative exchange, the air immediately adjacent to the surface of a human host is heated by conduction through the skin. That heated air is, in turn, transported by a variety of mechanisms. Bulk fluid motion convectively transports the heated air and, in natural environments, occurs in complex flow structures whose dynamics depend on the presence of objects and on the Reynolds number (a ratio of inertial to viscous stresses) and the Grashof number (a ratio of thermal buoyant forces to inertial forces). When bulk motion and inertia dominate (large Reynolds numbers) heat transport is dominated by forced convection. However, in still air, or in instances where the bulk motion is very mild, free convection dominates, and thermally induced buoyant plumes dominate heat transport (Campbell, 1977). In nature, both mechanisms are involved, leading to flow structures such as thermal plumes that rise and curl as they are transported downstream from the source.

Such convective plumes are characterized by a rise in centerline with distance from the source. The radius also expands with distance, and, when in a placed in a crossflow, the height of the plume is about one third the width of the plume. The rate of expansion varies with distance as a function of entrainment (Briggs, 1975, Huq and Stewart, 1996). As plumes rise, two counterturning-vortices are produced and propagate downwind. The vortices draw in surrounding air, dissipating the concentration of the plume. The rate of rising and entrainment are broken into two major regimes: near-field regimes are dominated by momentum, and far-field regimes are dominated by buoyant forces. The momentum dominated plume is often laminar or near-laminar, while the buoyant plume is often turbulent. Given this structure, one can develop hypotheses as to how the mosquito will behave in response to features of the plume structure. For example, downwind from the source, signal strength, and therefore responses, will be slight, given the dissipation and turbulence in this portion of the plume. Meanwhile, upwind flights exhibit more robust responses, assuming of course, that the mosquitoes target the highest concentrations (or perhaps least turbulent parts) of the plume.

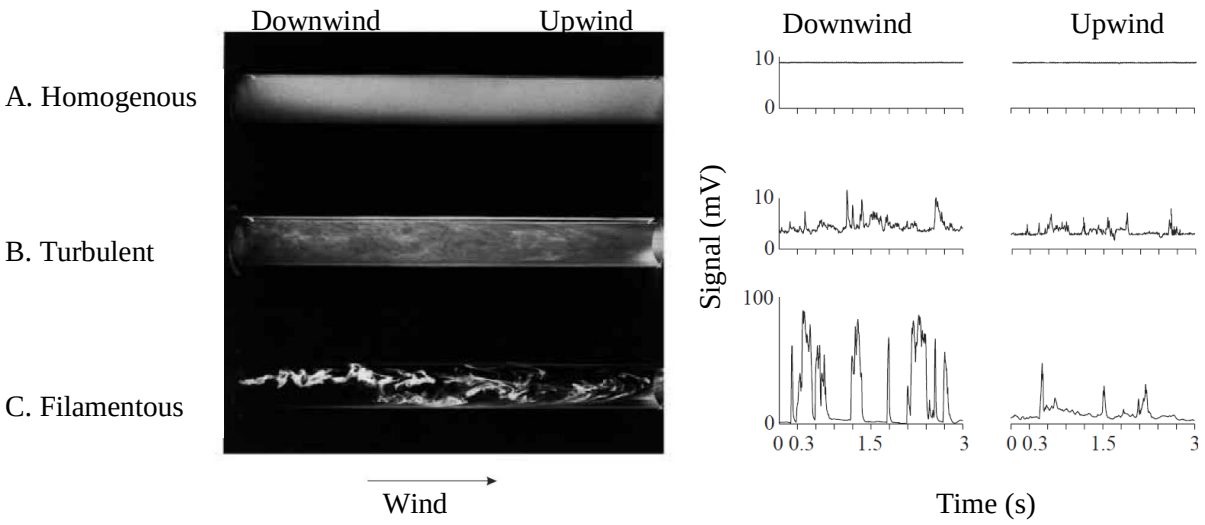

Figure 1.2 – Spatiotemporal features of flow regimes. A) Homogenous plume is imaged using $TiCl_4$ smoke (left) and smoke densities measured using changes in digital light signal at upwind and downwind locations. Recreated from Geier, Bosch and Boeckh, 1999, *J Exp Biol*.

In addition to heat transport, mass transport of water vapor, CO_2, and other chemical cues occur in spatially and temporally complex plumes. Thus the natural windborne signal a mosquito must follow is dynamic and difficult to predict. Windborne cues propagate through the environment as plumes, often mixing such that concentration does not scale linearly with distance from the source (Farrell et al., 2002). The movement of these plumes through a mosquito's outdoor habitat is dictated by environmental features, such as 1) the shape of the bluff body source, such as a human, 2) turbulent advection, primarily driven by wind pushing past large structures, such as flora and buildings, and 3) diffusive properties of the windborne particles. Also, the host-prey could be mobile, creating a meandering plume, which is then subjected to the mentioned environmental features. Altogether, these features can produce a highly spatiotemporally complex signal from which the mosquito gleans information about its host-prey.

Plumes presented in behavioral experiments are usually one of four types: homogenous, turbulent, filamentous, and laminar (van Breugel et al., 2015, Farrell et al., 2002, Dekker and Cardé, 2012, Cardé and Willis, 2008). Homogenous plumes have a uniform concentration, and, other than wind flow, have no spatiotemporal dynamics of the signal, such as a concentration gradient (Figure 1.2A). Homogenous plumes are achieved with high Reynolds numbers, produced via high rates of injected flow and high advection. Turbulent plumes occur at lower Reynolds numbers, the concentration of the signal is unevenly distributed, with regions of higher concentrations alternating with lower ones. These regions are largely produced by eddies that result from a dominance of shear forces in the flow, resulting in a signal with some temporal variance. While no smooth gradient exists, there is a time-averaged trend of decreasing concentration and increasing dispersal with distance from the source (Figure 1.2B).

Filamentous plumes are described by an uneven distribution of concentrations, usually with spatially correlated components (filaments), which propagate though the environment, resulting in signal with high temporal variance. There is no smooth gradient in this plume, but time averages of the plume are dispersed and diluted with distance from the source (Figure 1.2C). Laminar plumes are described by continuous and near-constant concentrations, which propagate through the environment with no mixing, and very little diffusion, if any. Laminar plumes may have a very slight smooth gradient up the centerline, but time averaged and instantaneous measurements of the plume are nearly identical.

4. Plume Navigation in Mosquitoes

Any time a mosquito navigates a plume, the behavior must change in response to the signal as well as the non-signal features of the flow, such as wind speed and direction. For example, in a turbulent plume, a mosquito may respond not only to the intermittency of the signal, but also the perturbations from the wind on a moment-to-moment basis.

Properties of flight and signal encoding together may increase the chance of detecting windborne host-prey signals. In most plume-tracking insects, the search behavior can be discretized into two modes of behavior: crosswind, oscillatory search, or *casting*, and upwind, direct flight, or *surging* (Cardé and Willis, 2008). It is believed that surging and casting are used in sequence to execute fast, accurate plume searches. While the surge-cast strategy appears in mosquito flight, it does not universally apply to mosquito flight, as their flights are oscillatory throughout, and seem to have differing behavioral regimes with a given plume type (Farrell et al., 2002). For example, casting is robust when mosquitoes are presented a laminar CO2 plume (Dekker and Cardé, 2012). Such idealized behavioral policies may be energetically taxing, resulting in execution of signal-following behavior varying with the signal type or intensity. It may be that the inconsistency of behavioral policy seen in mosquitoes may be driven by features of the plume, and signal type.

There are typical flight behaviors that the mosquito exhibits in the absence of host-seeking cues. For example, when presented with a constant wind speed, mosquitoes have a tendency to fly upwind. Flight behaviors that are not involved in search have been investigated on a small scale, to show that mosquitoes minimize drag forces by keeping their body axis parallel with the flow of the wind. To accomplish this feat, they often sideslip, a lateral translation of the body in space, achieved by rolling without yawing (Iams, 2012). This behavior increases stability during flight, which allows the mosquito more precise control of its flight trajectory. The act of laterally translating also keeps the mosquito in the same orientation relative to wind velocity, which may influence sampling or exposure to host signals.

The behavioral strategy of mosquitoes is known to change with encounters of host-prey signals. When presented with a brief presentation of CO_2, mosquitoes increase the probability of initiating flight,

and increase flight speed (Gibson and Carde, 2010). CO_2 presentations are also known to sensitize mosquitoes to skin odors and heat (Dekker et al., 2005, McMeniman et al., 2013).

Geier et al. investigated the effects of plume structure (homogenous, turbulent and filamentous) on the flight behavior of *Aedes aegypti* and found that, with CO_2 plumes, increased intermittency increased the likelihood of sustained upwind flight. That is, the more turbulent the plume, the less likely it is to see upwind flight. In contrast, the authors found that *Ae. aegypti* exhibit upwind flight in homogenous plumes of lactic acid, and argue that homogenous plumes may be most similar to the naturalistic structure of lactic acid plumes shed by humans. CO_2 plume navigation behaviors in laminar flows show an increase in crosswind oscillations, similar to the above-described casting behavior (Dekker, Carde, 2011).

5. Proposed Experiments

Here, I present a series of experiments to explore how the mosquito *Aedes aegypti* (Linnaeus, 1762) behaviorally responds to thermal signals. For the first time, I show how mosquitoes respond to convective thermal signals alone, and posit what features of convective thermal plumes are exploited in host-prey localization. First, I will discuss a detailed description of the convective thermal plume behavior in the wind tunnel. Second, I will describe behavioral responses to lateralized convective thermal plumes in a controlled environment. I will compare features of the flight trajectories to discern if and how mosquitoes' behaviors respond to the presence of plumes. By modelling gross plume structure and statistics, and seeing how they vary with flight dynamics, one can determine what features of the stimulus are behaviorally relevant. Finally, to measure this relationship, I will develop a computational model that incorporates statistics and features of the plume, as well as the measured behavioral responses to infer potential behavioral policies mosquitoes employ to navigate toward a thermal plume source.

References

van Breugel, F., Riffell, J., Fairhall, A., & Dickinson, M. H. (2015). Mosquitoes Use Vision to Associate Odor Plumes with Thermal Targets. *Current Biology*.

Altner H and Loftus R (1985) Ultrastructure and function of insect thermo- and hygroreceptors Annu Rev Entomol 30 273-295

Bowen, M. F. (1991). The sensory physiology of host-seeking behavior in mosquitoes. *Annual review of entomology*, *36*(1), 139-158.

Briggs, G. A. (1982). *Plume rise predictions* (pp. 59-111). American Meteorological Society.

Campbell, G.S. (1977. Attenuation of Radiation. *An Introduction to Environmental Biophysics*. Heidelberg Science. 157.

Cardé, R. T., & Gibson, G. (2010). Host finding by female mosquitoes: mechanisms of orientation to host odours and other cues. *Olfaction in vector-host interactions*, 115-142.

Cardé, R. T., & Willis, M. A. (2008). Navigational strategies used by insects to find distant, wind-borne sources of odor. *Journal of chemical ecology*, *34*(7), 854-866.

Dekker T, Geier M, Cardé RT. (2005). Carbon dioxide instantly sensitizes female yellow fever mosquitos to human skin odours. *Journal of Experimental Biology*. **208**:2963-2972.

Farrell, J, Murlis, J, Long, X, Li, W, Cardé R. (2002). Filament-Based Atmospheric Dispersion Model to Achieve Shor tTime-Scale Structure of Odor Plumes. *Environmental Fluid Mechanics*. **2** (1-2).

Ghaninia, M. (2007). *Olfaction in mosquitoes* (Vol. 2007, No. 93).

Grant, A. J., Aghajanian, J. G., O'Connell, R. J., & Wigton, B. E. (1995). Electrophysiological responses of receptor neurons in mosquito maxillary palp sensilla to carbon dioxide. *Journal of Comparative Physiology A*, *177*(4), 389-396.

Grant, A. J., & O'Connell, R. J. (2007). Age-related changes in female mosquito carbon dioxide detection. *Journal of medical entomology*, *44*(4), 617-623.

Gingl E, Hinterwirth A, Tichy H. (2005). Sensory representation of temperature in mosquito warm and cold cells. *Journal of Neurophysiology*. **94**.

Hay, S. I., Guerra, C. A., Tatem, A. J., Noor, A. M., & Snow, R. W. (2004). The global distribution and population at risk of malaria: past, present, and future. *The Lancet infectious diseases*, *4*(6), 327-336

Huq P, Stewart E. (1996). A laboratory study of buoyant plumes in laminar and turbulent crossflows. *Atmosphere and Environments*. **30** (7).

Maekawa E, Aonuma H, Nelson B, Yoshimura A, Tokunaga F, Fukumoto S, Kanuka H. (2011). *Parasites and Vectors*. **4**:10.

McIver S. (1973). Fine structure of antennal sensilla coeloconica of culicine mosquitoes.

Peterson, D. G., & Brown, A. W. A. (1951). Studies of the responses of the female Aedes mosquito. Part III. The response of Aedes aegypti (L.) to a warm body and its radiation. *Bulletin of Entomological Research*, *42*(03), 535-541.

Tichy, H., Fischer, H., & Gingl, E. (2008). Adaptation as a mechanism for gain control in an insect thermoreceptor. *Journal of neurophysiology*, *100*(4), 2137-2144.

Wang, G., Qiu, Y. T., Lu, T., Kwon, H. W., Jason Pitts, R., Van Loon, J. J., ... & Zwiebel, L. J. (2009). Anopheles gambiae TRPA1 is a heat-activated channel expressed in thermosensitive sensilla of female antennae. *European Journal of Neuroscience*, *30*(6), 967-974.

II.

Experimental Design and Plume Modeling

Abstract

The investigations described in this thesis were the first of a new research interest: exploring mosquito navigation in convective thermal plumes. With the goal of quantifying the neural mechanisms underlying host-seeking behavior in mosquitoes, this chapter explores the development, production and characterization of convective thermal plumes in a wind tunnel. Specifically, the development of a turbulent convective thermal plume, its measurements, and its spatiotemporal features are requisite to elucidate decision-making strategies in the mosquito during navigatory flight. To create the behavioral stimulus, two turbulent convective plumes were produced, each located in a lateral crosswind position in a wind tunnel, and radiative thermal energy was minimized. The plumes were made turbulent by the presence of a bluff body (the heating element) placed in the flow. The two plumes were found to be turbulent (Re = 630), but varied in temperature, rise height and dilution rates. Measurements of the plume revealed the existence of vortices that persisted along the length of the plumes. The plume behavior was also influenced by buoyant forces (Ri = 2.89). The plume centerline position and radius were well predicted by a numerical model of convective plumes in a crossflow, as seen on our wind tunnel.

Introduction

The relationship between behavioral output and sensory input often occurs in closed-loop, wherein the response of the animal or agent dictates the resulting available stimulus, and the stimulus detected influences behavioral output. With any behavioral study, one must have a confident estimation of the stimulus the organism encounters, if not full control of the stimulus in order to reveal the input-output relationship. It is often challenging, however, to simultaneously record free behavior in response to a natural stimulus. Many studies that solve this problem employ closed-loop systems in which a behavioral output is measured and used to update a controlled stimulus with small temporal delays (Suver, et al., 2012, van Breugel and Dickinson, 2012, Frye and Dickinson, 2004). Success of this strategy depends on a general knowledge of the behaviorally-relevant stimulus and a reliable, stimulus-dependent, behavioral response such as differential wing beat amplitude or body rotation. My research aims to describe behavioral responses of the mosquito to from approximately well-characterized stimulus, with aims to define behaviorally-relevant stimuli.

Characterizing turbulent plumes

The structure of plumes is dictated a combination of physical phenomena including inertial and viscous stresses and the strength of vorticity in a moving fluid. Convective thermal plumes introduce additional buoyant forces to a flow that can produce a plume of counterturning vortices that rotate and travel along the vertical axis of the plume. The entrainment rate, the rate at which surrounding air is mixed into the plume, can cause these vortices expand in diameter into the surrounding area. The entrainment rate, amount of rise of the plume, and turbulence vary with ratios of forces caused by viscosity, buoyancy and flow.

Many plume navigation studies characterize plume structure using a variety of visualization methods including a light vaporizing solid, such as TiCl4 or aerosolized fluids, such as fog (Willis et al., 2011). The densities of such particulates are presumed to be similar enough to air that they ad can be used as adequate proxies for plume behavior (Farrell et al., 2002). Statistics of the plume can also be captured using point measurements of concentrations, with the advantage of having temporally accurate measurements of intermittency, or variance of signal presence (Geier et al, 1999, Dekker and Cardé, 2011). Temperature in a thermal plume can be measured in the same fashion as volatilized plumes, as warm air moves through the environment in a similar--though, because of buoyant forces, not identical,--fashion to concentrations of airborne particles and gases.

Many behavioral experiments that investigate plume tracking behavior use laminar flows, to provide an easily-controlled, measureable stimulus (Lacey and Cardé, 2010, Farrell et al., 2002). This simple stimulus profile allows for a clear determination of plume boundaries, and clear delineation of plume-related behavior. However, such plumes may not represent the spatiotemporal structure of naturally occurring sparse, turbulent plumes (Willis et al., 1994). Further, mosquitoes are known to react differently to different plume structures (Geier et al., 1999). Thus, studying navigation behaviors using only laminar stimuli will not completely illustrate how spatiotemporally sparse windborne stimuli are computed to predict plume sources.

Here I describe the methods of producing the plume, measurements and verifications of constraints and features of a strictly convective thermal plume, and describe features of the plume using a model and point measurements in the wind tunnel volume. I use a numerical model to predict the shape of the plume, and use a series of point measurements to determine temporal features of the thermal signal, which could be used to provide spatiotemporal description of a convective thermal plume.

Development of Experimental Paradigm

This study explicitly asks whether mosquitoes use convectively transported heat in host-prey seeking behavior. The thermal attractive behaviors of mosquitoes seem more well-established anecdotally than scientifically investigated. As such, it is unclear what type of thermal energy is detected during searches. As mentioned in Chapter I, heat is transported by three mechanisms: 1) *conduction*, the transfer of thermal energy via adjacent materials, 2) *convection*, the transfer of thermal energy via moving fluids and, 3) *radiation*, the transfer of energy via photons. When heated objects are used in mosquito behavioral experiments, they typically emit a combination of radiative and convective heat (Lacey and Cardé 2010, McMeniman, et al., 2014) with conduction limited to the lamina of air immediately adjacent to the host.

To my knowledge, there are only a select few experiments that first sought to separate the various types of thermal energies available to mosquitoes. Peterson and Brown (1951) found that radiative wavelengths do not stimulate thermal attraction in female mosquitoes, and also showed that surfaces of varying radiative emissivities did not elicit a significant difference in attractiveness (measured by landing events). The authors conclude that mosquitoes must therefore be attracted to convective signals, and posit that radiative energy plays no role in attractive behaviors. Additionally, Gingl et al. (2005) tested the sensitivity of thermosensors to radiative and convective heat. They calculated that mosquito thermosensors, because of their geometry, are less sensitive radiative energy. Given that radiative energy decreases exponentially with distance, it is likely that convective thermal energy is a salient cue for mosquitoes' host-prey thermonavigation at moderate distances, (0.5 - 1 m).

To test for effects of only convective thermal plumes, one must produce a thermal plume from a source with minimal radiative emissivity. There are various traits which cause changes in radiative emissivity such as roughness and thickness of surface. By manipulating the surface element and smoothness, one cane augment the radiative emissivity of a thermal source. Here, we used polished gold leafing to minimize radiative

Characterizing and Producing Convective Plumes

Thermal plumes can be produced in two ways: *natural* (or free) *convection*, the production of flows and plumes resulting from temperature-dependent changes in fluid density (buoyant forces), and *forced convection*, the production of flows and plumes from air forced – by some mechanism other than heat – over a warm surface. The plumes in the wind tunnel contain both forced and natural convective energies. In order to accurately model the plume structure, the dominant energy must be determined. Natural convective thermal plumes are often turbulent, due to buoyancy and added (thermal) energy into the fluid system. The buoyancy of the thermal plume may be a salient behavioral signal, so eliminating it from the environment, as with a strictly forced convective plume, may produce behaviors that are not naturalistic.

In order to approach the complex statistics of naturalistic thermal signals, I produced a buoyant, turbulent plume in a wind tunnel, containing both natural and forced convection.

Understanding features of the plume is critical for determining the behaviorally relevant thermal stimuli mosquitoes detect in host-seeking. Measurement limitations of turbulent thermal plumes make it exceedingly difficult to characterize the spatiotemporal patterns of instantaneous temperatures throughout the volume as mosquitoes are navigating these complex structures. Instead, I used a combination of instantaneous point measurements of temperature and models of thermal convective plumes to calculate the time-averaged spatiotemporal patterns and plume geometry, respectively. With this reasonable estimate of the plume, I can explore thermal correlates of mosquito trajectories in the plume.

Interactions of Buoyant and Drag Forces

To my knowledge, the effect of heated, vertically-oriented cylinders on flows has not been well described, and the potential interaction between buoyant and drag forces is complex. Drag forces are a result of viscous and pressure stresses. Wakes behind bluff bodies are a consequence of viscous energy dissipation and lead to a pressure gradient associated with flow separation around the body. The extent to which pressure and viscous stresses contribute to the total drag and the geometry of the resulting wake depend on the Reynolds number. In a wide range of Reynolds numbers ($\sim 50 - 10^5$), wakes are dominated by vortices alternately shed from either side of the cylinder, resulting in a Karman vortex trail. At very high Reynolds numbers ($> 10^5$), a turbulent wake persists several length scales downstream of the structure (Vogel, 1994).

The thermal energy introduced into a closed, dynamic system produces buoyant forces. The resultant vertical velocity can produce stable, counter-rotating vortices, which entrain air first from upwind of the source, then normal to the plume centerline as it rises. Mushroom clouds after an awesome and majestic explosion are a large-scale example of such vortex structures. In the case of a buoyant force in a cross flow, as occurs in these experiments, the vortices are propelled downwind, and entrainment becomes normal to the plume centerline with downwind propagation and elevation.

There is concern that the downwind propulsion of these vortices may interact or be influenced by the drag-induced Karman vortices. However, in the case of a heated vertical cylinder, the buoyant forces act to suppress Karman vortices, and may reduce drag forces acting on a cylinder by reducing the width of the wake immediately downstream of the body (Noto and Fujimoto, 2007). To understand this phenomenon, consider an air particle moving through the wind tunnel, at the height and near the centerline of the cylinder. As the particle nears the heater, it is warmed and begins to rise as the fluid becomes less dense. Instead of passing around the cylinder, parallel to the floor of the wind tunnel, buoyant forces lift the particle such that it travels up along the circumference at an angle. The particle,

starting at the height of the heater, may likely be above the height of the cylinder once it has downwind of the diameter, and becomes entrained in one of the buoyant vortices. Given these properties of interaction, one can expect a buoyant plume model to describe well the features of the plume.

Predicting Buoyancy Curves, Length Scales, and Dissipation Rates of the Thermal Plume

A convective thermal plume will have a vertical, buoyant curve, largely driven by differences in density between the introduced stream and the freestream flow, as well as the mean rate of freestream flows. Below I calculate vertical features of the plume by treating the air warmed by the heaters as an injected flow, with a mean velocity equal to that of the freestream, and density calculated at the heater's hottest surface temperature.

Materials and Methods

Experiments were carried out in a custom-built wind tunnel, with a 1 m x 0.26 m x 0.26 m Plexiglas working section. Wind speed was kept at a constant 0.5 ± 0.05 m s^{-1}. For all measurements taken in the wind tunnel, the heaters were held in position, each placed 0.15 m downwind from the intake screen, 0.72 m from each side walls, and 0.38 m from the floor of the working section. In the downwind portion of the wind tunnel, the mount for the mosquito holder cage was present (0.03 m x 0.03 m x 0.09 m, depth x width x height, respectively).

A turbulent plume was produced by placing the cylindrical heating rods (0.8 cm length, 0.06 cm diameter) in the wind tunnel. To produce a thermal stimulus, one of the heaters was held at 50.0 ± 0.1 C using a PID controller (Watlow EZ-ZONE PM Express).

. The vortex shedding produced by thermal energy and bluff bodies in the cross flow introduced shear forces, and thus turbulence, into the environment, while the laminar flow of the wind tunnel provides control of general structure of the plume, allowing for some repeatability. Turbulence was minimized by mounting the heaters in 3D-printed, heat tolerant, airfoil-shaped holders.

Filtering Out Radiative Thermal Energy

The heating rods used for experiments are made of a nickel-based alloy, Incoloy 800 (Special Metals Corporation). The Incoloy heating rod has a low radiative emissivity ($\varepsilon = 0.20$), at 250 W. I covered the heaters with gold leaf, to further reduce radiant energy loss. The radiant energy loss of the heater was calculated for both the bare and gold-leafed heaters. I measured emissivity using an infrared camera (FLIR AS325sc), and the emissivities were measured using proprietary infrared measuring software (FLIR ExaminIR).

There is a possibility of radiative signals emitting from the plastic holders or other plastic components of the wind tunnel. Most plastic materials have high radiative emissivities, often assumed to be $\varepsilon = 0.95$. For the heater holders to emit detectable levels of radiative energy, they must be warmed to at least 199.54 °C. Thus, we assume the plastic surfaces do not sufficiently produce detectable radiative thermal energy.

Characterizing the Plumes

Three dimensionless numbers characterize the flow. The Reynolds number (*Re*) is the ratio of inertial to viscous stresses in a moving fluid and is often used to estimate conditions in which flows transition from laminar to turbulent structures. Reynolds number is inversely proportional to the fluid kinematic viscosity (ν), and directly proportional to the flow speed (*U*) and a characteristic length (*L*):

$$Re = UL/\nu \tag{2.1}$$

When the Reynolds number is large, inertial forces dominate and vorticity and instabilities can lead to turbulence. At low Reynolds numbers, viscous energy dissipation dominates and turbulence is unlikely.

The Grashof number (*Gr*) is a ratio of the product of buoyant and inertial forces to the square of viscous forces:

$$\mathrm{Gr} = \beta g L^3 \Delta T/\nu^2 \tag{2.2}$$

where β is the coefficient of thermal expansion, g is gravity, and ΔT is the temperature difference between the air and the heated surface. The Grashof number thus represents the influence of buoyant forces driving bulk motion, inertial forces associated with that bulk motion relative to the restraining effects of viscous forces. At very low Grashof numbers thermal changes in fluid density become significant drivers of bulk motion. Finally, Richardson number (*Ri*) is used to determine if buoyant forces or inertial forces dominate. The Richardshon number is the ratio of Grashof number to the square of the Reynolds number:

$$Ri = Gr/Re^2 \tag{2.3}$$

Buoyancy dominates flows where Ri > 10, whereas forced convection (bulk flow) dominates at $Ri < 0.1$. Together, these dimensionless numbers (Reynolds, Grashof, Richardson) characterize the some of the mechanisms that contribute to plume structure.

Modeling the transverse, bent-over plume (Figure 2.1) produced by the heaters was modeled by following descriptions provided by Huq and Stewart (1996). Like most bent-over plume models, the Huq and Stewart modeled a forced convection using a jet or stack producing a stream of warm air into the environment. To apply this model to my system, I modeled the introduced flow using the equivalent of fire or flame sources, which are energy dependent and do not have constraints on spatial origins of the plume. Ranjan, et al., (2012) model features of a bent-over plume from a flame, and provide a calculation to show that the buoyant flux, *B*, based on energy release rate of the source, instead of buoyant:

$$B = \frac{g\dot{E}}{\rho c_p \Theta U}, \tag{2.3}$$

where Ė is the thermal energy release rate of the heater, ρ is the density of the freestream air, c_p is the specific heat at constant pressure, Θ is the absolute temperature of the freestream air, and U is the cross flow velocity. Table 1 shows the calculated values of this equation. The remainder of the model follows Huq and Stewart (1996). Air density was calculated as a function of temperature, pressure and humidity using customized MATLAB scripts.

Table 1 – Buoyancy plume parameters and calculation.

Symbol	Parameter	Value
Θ	Mean temperature (K)	294.65
U	Freestream velocity (m s^{-1})	0.50
P	Pressure (Pa)	1.00
c_p	Specific heat (kJ kg^{-1} K^{-1})	1.01
Ė	Heater wattage (W)	250
B	Buoyant flux (m^3 s^{-2})	1.18

Near the source, the plume is governed by momentum forces, and is laminar. As the plume propagates downwind, the shape is governed by buoyant forces, and dissipates, largely due to the entrainment constant. The length scales of these regions (l_m and l_b, respectively) can be used to determine the location at which this transition occurs. Entrainment can also determine dissipation rates of temperature within the plume. The relationship of vertical speed to cross-wind radius of the plume is used to calculate dissipation rate, ε_A of the plume. Here, the dissipation rate can be used to predict density along the centerline of the plume (Huq and Stewart, 1996). Variations in these values may arise due to decreased wind speeds and pressures formulated from vortex shedding around the cylindrical heating rod.

The buoyancy arc, length scale, and other features of the plume are fit to measurements taken within the plume (Figure 2.1).

Plume Measurements and Model Confirmation

To measure the plume at repeatable locations, a custom-designed measurement apparatus consisted of an array of four thermocouples and corresponding controllers, and a 3D printed thermocouple holder. Thermocouples were 0.13 mm diameter, T type wires (Omega), with a 0.04 s response time (18 C to 37 C test range). The thermocouple array was moved throughout the volume of the working section, and recordings were taken at least 480 unique positions. Time-average recordings at these positions are shown in Figure 2.2A.

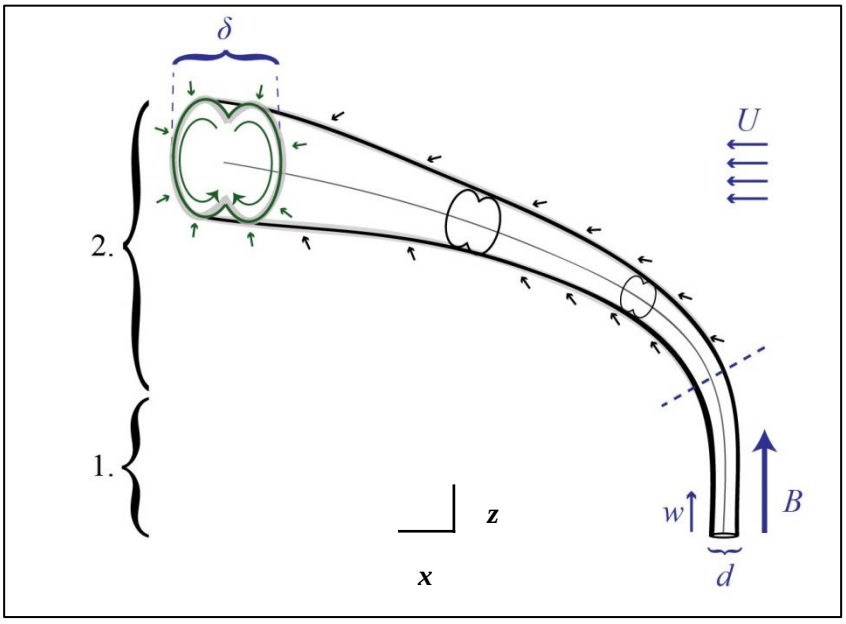

Figure 2.1 - Schematic of predicted thermal plume in crossflow. Buoyant plumes in a crossflow are considered bent-over plumes. Bent-over plumes can be segmented into two regimes. ***1***) The momentum-dominated regime occurs near-field, with $z \sim x^{2/3}$, and ***2***) the buoyant dominated regime occurs far field, with $z \sim x^{1/3}$. The transition of regimes occurs at the critical point indicated by the dashed line. Location of the critical point is determined by the ratio of upward velocity, ***w,*** entrainment rates (not shown) and initial differential temperature, ΔT. Plume shape is governed by the diameter at the source, ***d***, the buoyant flux, ***B***. The rising rate and radius ***d***, are governed by the ratio of the freestream velocity, ***U***, and **B**. Radial expansion is driven largely by height of the centerline (gray line) and entrainment of air (black arrows). The ratio of horizontal width to vertical width is approximately 3:1. Two counter-turning vortices are formed and propagate downwind (green arrows).

The thermocouples were held in a fixed, linear orientation, 30 mm apart from one another in the 3D printed thermocouple holder. The holder was mounted on a metal post, the bottom of which has a strong magnet fixed into the bottom. A paired magnet was placed underneath the floor of the working section so the apparatus could be moved through the volume with minimal disturbance of flow (Figure 2.2B). The

vertical height of the array was adjusted by swapping different length posts under the array. Temperatures were measured at two vertical heights.

Measurement locations were placed at vertices of a grid that was laid out along the floor of the wind tunnel, which held markings that were 1.905 cm wide (crosswind dimension) by 5 cm long (upwind dimension). Given that mean temperature and variance decrease with distance from the plume source, measurement locations were densely sampled for crosswind half of the wind tunnel expected to contain the plume. Temperatures were digitally recorded for 20 seconds at each location, with a 500 Hz sample rate, using custom MATLAB scripts. Recordings were then downsampled to the Nyquist frequency, derived from the time constant of thermocouples (50 Hz). Time-averaged temperatures were produced by averaging over the total duration of recording, at Nyquist frequency. Spatial probabilities of temperatures were calculated binning the full range of measured temperatures for each plume into five equal-sized bins. Then, the number of occurrences of each temperature group was counted for each bin and normalized by the number of samples, producing a probability of temperature over the 20 s recording span.

Results

Filtering Out Radiative Energy

Layering the heaters with gold leaf effectively reduced the emissivity of the heaters from 0.20 to 0.10-0.12. Calculated irradiances can be found in Table 2.

Measured surface temperature of the holder was 21.36 °C. The air in the wind tunnel warms over time, reaching a steady state around 45 min. There was some concern that surrounding acrylic in the wind tunnel warms over time. Wall and ceiling temperature surrounding the heater were found to be 20.01 ± 1.02 °C, with average air temperatures of 19.15 ± 0.05 °C. The increase of thermal radiation from the surrounding acrylic would then be, with clear acrylic having an emissivity of $\varepsilon = 0.94$, is 7.40×10^{-8} mW cm^{-2}.

Table 2 – Radiative thermal energy measurements of the bare and gold-leafed heating rods.

Measurement	**Value**	
	Left Heater	**Right Heater**
Heater surface temperature (K)	306.85	309.75
Ambient temperature (K)	294.65	294.65
Absolute bare heater irradiance (mW cm^{-2})	10.05	10.44
Absolute leafed heater irradiance (mW cm^{-2})	5.35 – 6.03	5.22 - 6.26
Introduced leafed heater irradiance (mW cm^{-2})	0.75 - 0.90	0.95 - 1.13

Characterizing the plume

Dimensionless numbers in Table 3 indicate that the plume both natural buoyancy forces and forced convection forces (here, the wind tunnel airflow) contribute to the plume structure ($0.1 < Ri < 10$). Moreover, both the buoyancy length scale and the momentum length scale are of the same order of magnitude with each other, suggesting there are nearly equal contributions from both free and forced convective mechanisms. An entrainment constant, β, of 0.6, as standardized by Briggs (1984) provided the best approximation of the flow.

Table 3 – Dimensionless values of plumes

Symbol	Dimensionless number	Calculated Value
Re	Reynolds number	630
Gr	Grashof number	1.15×10^{6}
Ri	Richardson's number	2.89
l_M	Momentum length scale	5.8 x 10-3
l_B	Buoyancy length scale	4.5×10^{-3}
B	Entrainment rate	0.6

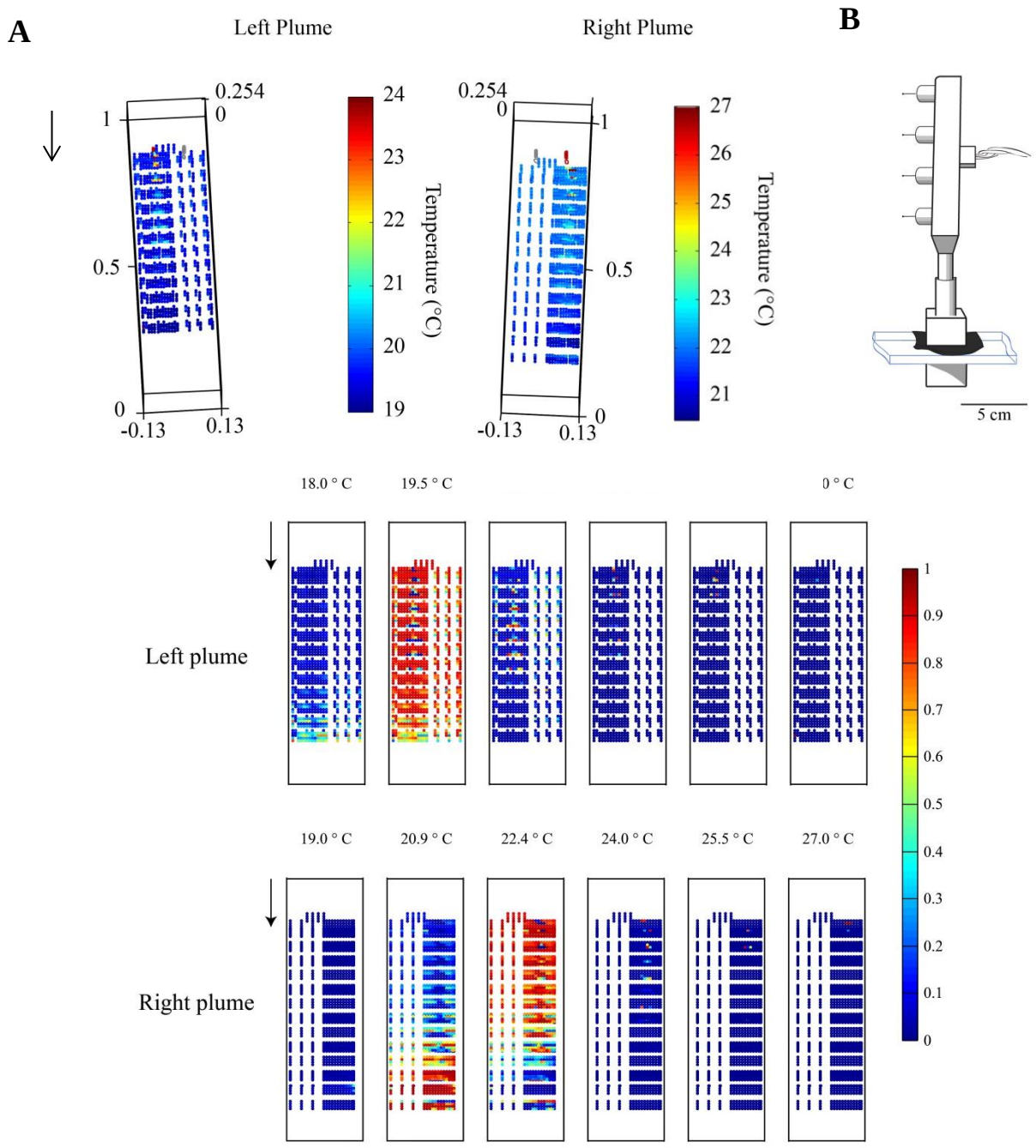

Figure 2.2 – Time averaged and spatial probability distribution of wind tunnel temperature. **A**) A scatter plot of temperatures averaged over 20 s, for both plumes. Heating elements are shown as gray (off) and red (warmed) cylinders. View presents data as crosswind slices through the volume. Color indicates temperature. The characteristic columnar vortex columns are seen in the right plume (right). B) Schematic of the thermocouple array. The magnetized bottom and holders, felt cover (black) are shown in place with Plexiglas (blue). **C**) Scatter plot of probabilities of binned temperature range. Temperatures were binned; bin center values are shown above each plot. Color indicates probability of given temperature. The left plume is cooler, but maintains a similar structure as right. The right plume has an apparent gradient along the long axis of the wind tunnel. Arrows indicate wind direction.

Plume Measurements

Time averages of measurements taken through the wind tunnel volume show warm regions exist downwind of the heaters (Figure 2.2A). The plumes have varying temperatures and heights, with temperatures increasing inversely with distance from the heater. Spatial probability distributions of temperature clearly show the vortex structure present in both plumes. Cooler regions extend away from the centerline of the plume, with concentrations of cool temperatures in the vortices. Warm air is concentrated along the centerline, between the two vortex structures. The warm downwind region occurs from averaging temperatures in that area before and after the flow reached a steady state.

Plume Model

Huq and Stewart (1996) compared the plume geometry of their model to empirical data, wherein they introduced a more dense fluid to a less dense flowstream, and used fluorescent dye introduced into the flow with the plume fluid. Visualization of the thermal plume in my experimental set up cannot easily be accomplished. Instead, verifications were made using time averaged temperature measurements, with plume boundary, rise, and width determined by the location of the warmest regions of the time-averaged measurements (Figure 2.2A). This form of measurement makes the measured plume smaller than the volume determined by entrainment, and includes regions of the wind tunnel that may be warm, but do not have spatiotemporal features of the plume. The area of the plume model includes regions that have low time-averaged temperatures, but are likely to have a temporally-varying warm signal.

Buoyant plumes in a laminar crossflow, such as the one in the wind tunnel, have a vertical profile, z, that rises as a function of downwind position, x (Figure 2.1). The plume can be segmented into two regimes: momentum-dominated and buoyancy-dominated. In the near-field, the rise of the plume, is such that $z \sim x^{1/3}$, whereas far-field, the plume rises such that $z \sim x^{2/3}$. The transition between these two regimes occurs at the length buoyant scale of the plume, l_B. The height of the maximum temperatures were measured along the centerline of the plume, and plotted as a function of distance (Figure 2.3A). I found that, as indicated by the Richardson number and the buoyant length scale, the majority of the plume rise and radii of the empirical plumes follow the ⅔ power law. The time-averaged temperature of the plume, however, does not capture features of entrainment near the boundary, where the average temperature is low, but instantaneous warm temperatures is still likely to occur. To avoid this error, verification of model and empirical plume radii was calculated by using the probability distributions of temperature through the wind tunnel volume by thresholding the distribution at 0.5 for each bin, measuring the crosswind width, and averaging across bins. The radii of the modeled plume and the empirical plume were found to follow the 2/3 power law, however the empirical radii were consistently larger than the plume radii at a given distance (Figure 2.3B).

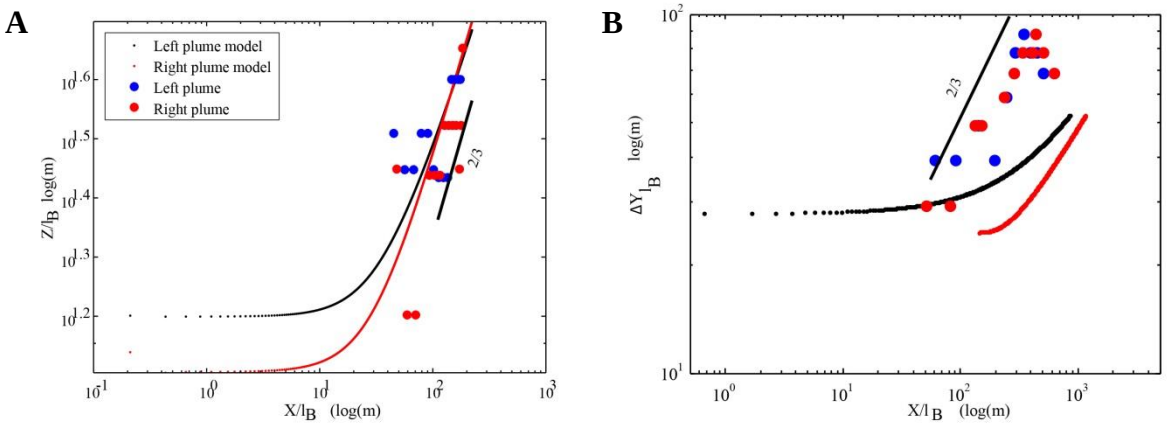

Figure 2.3 - Vertical rise and radius of the plume as a function of distance. **A**) Centerline heights of the plumes and **B**) radii of plumes are plotted against normalized distance from the source. Plume heights are vertical location of max temperature along the centerline of the plume. Small points are from model, larger points are measured data. Radii are measured from spatial probability measurements. The black bar indicates 2/3 power-law slope

The vertical profiles of mean density at the centerline show the change in concentration of the plume as a function of downwind progress. Huq and Stewart's experimental plume model used an injected fluid with a higher density than ambient. My calculations had to be adjusted in order to compare data and comparatively determine our plume regime. To recreate vertical profiles of mean density at the plume centerline as described by Huq and Stewart (1996), the densities were calculated from time averaged temperatures at various heights across the centerline. The density was non-dimensionalized by the initial density difference, $\Delta\rho_0$. These data were found to be roughly quadratic. The minima of each dataset were plotted as a function of distance, to get the dilution rate (Figure 2.4C). It was determined that the empirical plumes have trends similar to those seen in Huq and Stewart's laminar, though the slopes and therefore range of z/l_B values are different.

The centerline dilution ($\Delta\rho_0/\rho_{min}$) of the plume changes with the effects of turbulence. When comparing my data to that of Huq and Stewart (1996), the minimum density was used instead of max so the rates of centerline rise have the same signed slope as their data. (Figure 2.4C) The centerline dilution of the two plumes is similar to the laminar regime. Both plumes have a low dilution rate (left plume - 1 x 10^{-3}, right plume = 8.51 x 10^{-6}), with the right plume having a faster dilution rate than the left.

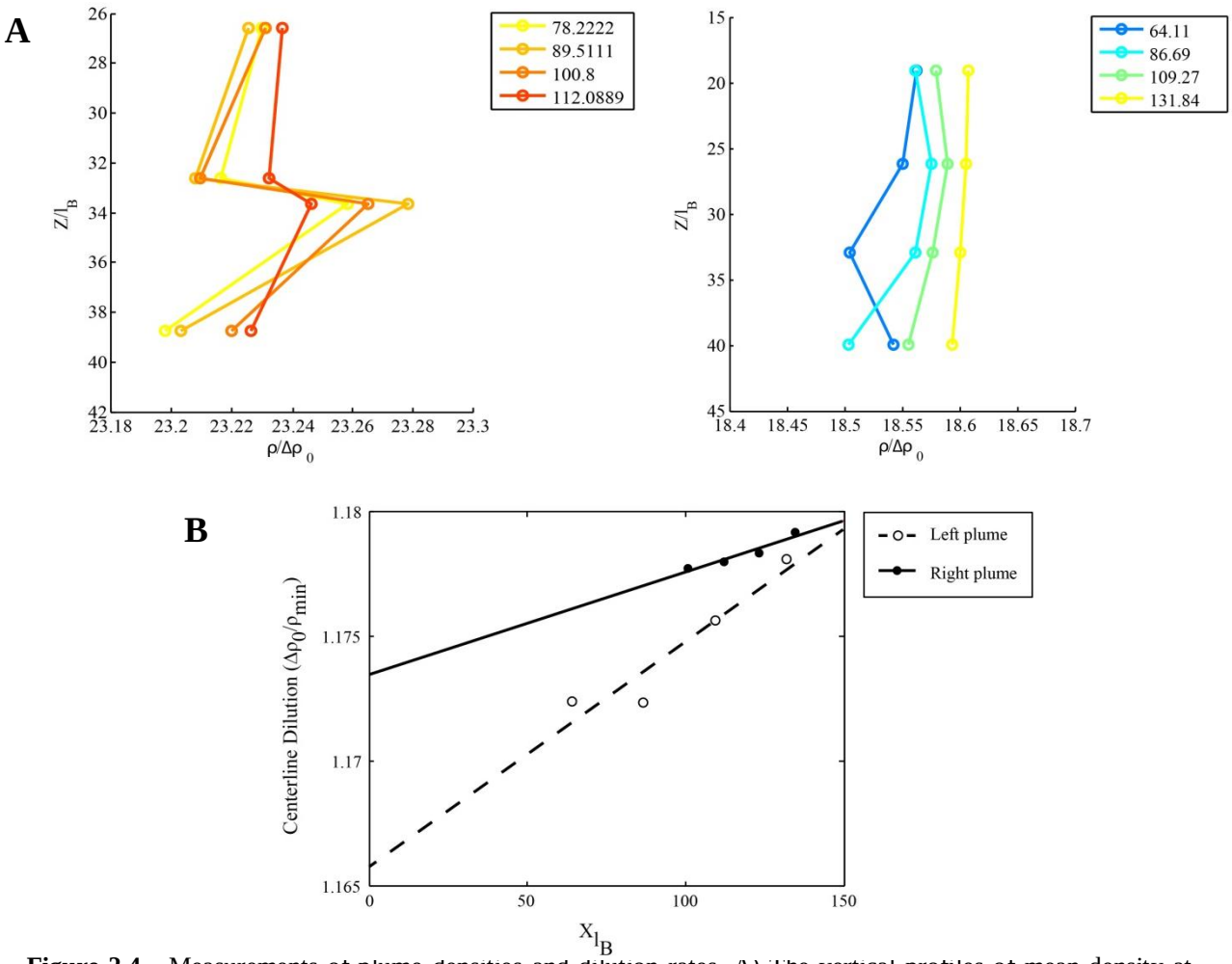

Figure 2.4 - Measurements of plume densities and dilution rates. A) The vertical profiles of mean density at plume centerline for the left and right plumes. Colors denote locations downwind. The mean density increases and spreads with distance, and the minimum values decrease in height with distance. **B)** Centerline rise and relation to downwind position developed from locations of minimum concentration. The rate of dissipation is higher in the left plume than the right, with the left plume having smaller differences in density, compared to the origin. The high dissipation rates could be due to the low position of the plume interacting with the cylinder wake.

Discussion

Filtering out radiative energy

Gingl et al. (2008) calculated the amount of radiative power required to evoke a change in spike rate in the thermosensitive neurons. They found that 1 spike s^{-1} change in firing rate could be evoked in warm cells change with a 1.21 $mWcm^{-2}$ stimulus, and, in cold cells, with a 1.11 $mWcm^{-2}$ stimulus. Given these data, and assuming a 1 spike s^{-1} change in spike rate does not reliably elicit behavioral changes, one can assert that, even if behaviorally relevant, the introduced radiative energy from the heaters is just insufficient to influence navigatory behaviors.

Just as demonstrated by Huq and Stewart (1996) the centerlines of the measured and predicted plumes were found to follow the 2/3 power law, as predicted (Figure 2.3A). The radii of the measured plumes were also found to follow the 2/3 power law. The distances were non-dimensionalized using the buoyancy length scale. The normalized distances where the 1/3 power law describes the plume behavior, in my experimental plumes, are too small to measure and were thus not available to comparison to the model. Thus the overall structure of the plumes can be described by the buoyant 2/3 power law. The radii were found to be slightly larger than the predicted values, however, this may be an artifact of measurement strategy, as radius measurements calculated from the time averaged temperature produced smaller-than-predicted values.

Given these calculations, I confidently assume that the surfaces in the wind tunnel, though heated, do not produce enough radiative power to be detected by the mosquitoes. The methods presented are ideal for producing a thermal plume in a wind tunnel. Two heaters were present in the tunnel at all times, with one or neither heated for any given behavioral trial. With constant visual cues and varying thermal stimuli, this setup is analogous to a y-maze. We can also observe flight behavior in an analogous fashion, measuring biases toward the warmed heating rod.

Characterizing the plume

I have found that the adjusted Huq and Stewart model is suitable for predicting the plume geometry, given the experimental setup. Figure 2.5 illustrates that the modeled plume boundary well-encompasses the time-averaged temperature measurements. Using this model allows one to adjust the plume

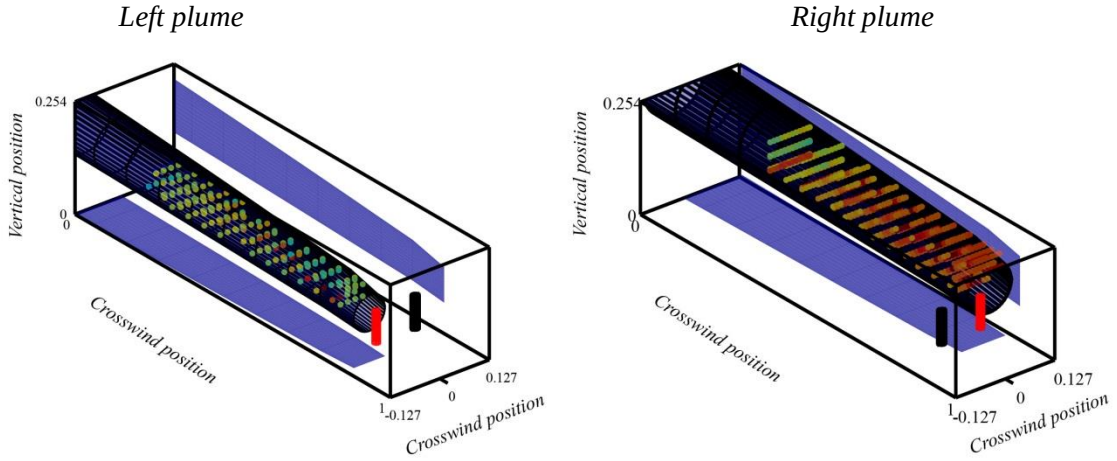

Figure 2.5 – Theoretically derived plume boundaries. Plume boundaries are shown in dark blue, with measured temperatures overlaid. Shadows of the plume are indicated to show vertical and crosswind positions. The warmest measured regions of the plume are fully encapsulated by the boundaries. The left and right plumes vary in mean diameter and height due to differences in surface temperature of the heating rods.

boundaries to the temperature changes seen in behavioral experiments. This plume also can be used in modeling mosquito behavior, providing boundary and mean temperatures of the plume.

Comparing the results of all measurements, models and calculations, allows one to make approximate claims about features of the thermal plume, and predict dynamics. There are a few differences between the Huq and Stewart experimental methods, which affect the application of their measurements to this data. Huq and Stewart generated their plume by introducing a dense fluid into a crossflow from above. The change in height is therefore the inverse of the measurements from a thermal buoyant plume. The rate of change of density with also differs; the authors measured the decrease in density, while I measured the increase. Finally, the scale of their plume is far larger than mine, resulting in a different range of dimensionless downwind (x/l_B) values. These differences make it difficult to successfully compare my plumes to theirs, especially in the momentum-dominated region. Their model remains applicable, as the many of the measures are unitless, and the buoyant-dominant region was still predicted

One potential drawback of this model is the lack of bluff body effects in the flow. The drag forces induced by the heated cylinder, though suppressed by buoyant forces, may still influence the geometry of the plume. The mixing region in the near-field may have higher entrainment rates or patterns than the model predicts. Measurements of the plume showed warm regions at lower elevations than the model predicted. To include these regions in the plume, the model boundary was elongated in the vertical dimension, following a 3:1 vertical to horizontal ratio often seen in bent-over plumes (Hoult Fand Weil, 1972). Another example of a bluff body affecting the plume is evidence of a slight crosswind meander to the plume, presumably caused by Bernoulli's effect. The placement of the heaters near the wall is likely to have created a lower pressure region between the heater and the wall, driving the plume toward the walls. This is seen as a 0.01 m shift in centerline near the heated cylinders. The shift is very small, and the modeled plume boundaries still encompassed these warm regions.

It is important to note the distinction between the left and right heaters. Though programmed to produce the same temperature, the left heating rod surface temperature was consistently lower than that of the right heater. This difference resulted in different plume heights, widths, and temperatures, and lower dilution rates, as seen in Figure 2. Evidence of the counter-turning vortices can be seen in cross sections of the time-averaged right plume, but are absent in the time-averaged left. However, the vortex structure of the left plume can be seen in the spatial probability maps of varying temperatures, suggesting that the intermittency of the plume is affected by vortex behavior. The behavioral experiments can be used to investigate not only how mosquitoes respond to the plume, but also changes in plume structure governed by differences in temperature.

The temperature measurements and plume model illustrate that the structure of the plume is well described as a bent-over buoyant plume, and the plume structure is dictated by buoyant forces and related vortices. I have also shown that the plume is turbulent, with centerline height and radius that follows a 2/3 power law, despite the plumes being different temperatures and therefore diameter. The boundaries of the plume can be described by the Huq and Stewart model, although the radii of the model are slightly larger than the probability-derived empirical radius.

These features can help inform predictions of mosquito behavior. For example, one can consider the vortex structure as informative regions, where the distance between two warm regions within the plume cross-section, dictates the distance from the source. The bent-over buoyant plumes may likely have a region of turbulence along the top of the shape, where entrainment directions converge, and the ceiling boundary layer may affect mixing in the structure. This feature was not measured, but is often seen in bent-over buoyant plumes (Hoult and Weil, 1972). Thus, we can anticipate seeing behavior that exploits these warm vortices as well as the mixing area along the top, as these two positions will change with the height and distance from the source. Because they are equipped with thermosensors which encode change in temperature, and because the probability of a range of temperatures changes with upwind position, a mosquito may also detect features of the plume based on the distribution of different temperatures in a given position.

Altogether, this methodology offers an effective way to control thermal energy in behavioral setup, while the model presents a powerful, dynamic tool for predicting complex plume structure in a controlled environment. We have an approximation of a handed plume that is presented in a y-maze fashion, allowing us to observe navigation behaviors without corresponding visual cues. Such information will hopefully encourage the use of spatiotemporally complex signals in mosquito behavioral experiments, which will help elucidate behavioral strategies to naturalistic, complex windborne host signals.

References

van Breugel, F., & Dickinson, M. H. (2012). The visual control of landing and obstacle avoidance in the fruit fly Drosophila melanogaster. *The Journal of experimental biology*, *215*(11), 1783-1798.

van Breugel, F., Riffell, J., Fairhall, A., & Dickinson, M. H. (2015). Mosquitoes Use Vision to Associate Odor Plumes with Thermal Targets. *Current Biology*.

Dekker T, Cardé RT. (2011). Moment-to-moment flight manoeuvres of the female yellow fever mosquito (Aedes aegypti L.) in response to plumes of carbon dioxide and human skin odour. *Journal of Experimental Biology*. **214**.

Farrell, J, Murlis, J, Long, X, Li, W, Cardé R. (2002). Filament-Based Atmospheric Dispersion Model to Achieve Shor tTime-Scale Structure of Odor Plumes. *Environmental Fluid Mechanics*. **2** (1-2).

Frye, M. A., & Dickinson, M. H. (2004). Closing the loop between neurobiology and flight behavior in Drosophila. *Current opinion in neurobiology*, *14*(6), 729-736.

Geier M, Bosch, O, Jurgen B. (1999). Influence of odour plume structure on upwind flight of mosquitoes towards hosts. *Journal of Experimental Biology*. **202**.

Gingl E, Hinterwirth A, Tichy H. (2008). Sensory representation of temperature in mosquito warm and cold cells. *Journal of Neurophysiology*. **94**.

Hoult, D. P., & Weil, J. C. (1972). Turbulent plume in a laminar cross flow.*Atmospheric Environment (1967)*, *6*(8), 513-531.

Huq P, Stewart E. (1996). A laboratory study of buoyant plumes in laminar and turbulent crossflows. *Atmosphere and Environments*. **30** (7).

Lacey ES, Cardé RT. (2010). Activation, orientation and landing of female Culex quinquefasciatus in response to carbon dioxide and odour from human feet: 3-D flight analysis in a wind tunnel. *Medical and Veterinary Entomology*. **25**.

McMeniman C, Corfas R, Matthews B, Ritchie S, Vosshall L. (2014). Multimodal integration of carbon dioxide and other sensory cues drives mosquito attraction to humans. *Cell*. **156**.

Noto K, Fujimoto K. (2007). Numerical computation for buoyancy effect on three-dimsnionalty and vortex dislocation in heated wake with vertical mainstream. *Numerical Heat Transfer, Part A: Applications: An International Journal of Computation and Methodology*. **51** (6).

Peterson DG, Brown AWA. (1951). Studies of the responses of the female Aedes mosquito. Part III. The response of Aedes aegypti (L.) to a warm body and its radiation. Bulletin of Entomological Research. **42** (3).

Ranjan P, Perez K, Alvarado T, Potter B, Breidenthal RE (2014). Chemically-reacting, transvers plume. University of Washington Aeronautics & Astronautics Report.

Suver, M., Mamiya, A., Dickinson, M.H. (2012). Octopamine neurons mediate flight-induced modulation of visual processing in *Drosophila*. *Current Biology.***22** (24).

Vogel S. (1994). Life in moving fluids: The physical biology of flow. Princeton Paperbacks.

Willis M, David C, Murlis J, Cardé R. (1994). Effects of pheromone plume structure and visual stimuli on the phermon-modulated upwind flight of male g**** moths (*Lymantria dispar*) in a Forest (Lepidoptera: Lymantriidae). *Journal of Insect Behavior*. **7** (3).

Willis, M. A., Avondet, J. L., & Zheng, E. (2011). The role of vision in odor-plume tracking by walking and flying insects. *The Journal of experimental biology*, *214*(24), 4121-4132.

III.

Behavioral Evidence of Convective Plume Tracking during Flight in The Mosquito (*Aedes aegypti*)

Abstract

The yellow fever mosquito (*Aedes aegypti*, L.) is attracted to warm air and surfaces, and presumably thermonavigates using inputs from the pair of thermosensors found at the distal ends of their antennae. How they thermonavigate is contingent on the type of thermal energy they actively detect, as convective thermal signals are heterogeneous, while radiative signals produce a smooth gradient through space. This study investigates the interactions between mosquitoes and convective—but not radiative-- thermal signals in a wind tunnel. We investigated the behavioral response of female mosquitoes to the presence of a lateralized thermal plume (left or right), when radiative energy is below detectable levels. We show for the first time that mosquitoes strongly bias their flight toward the plume-side of the wind tunnel ($p < 0.01$). The bias is elicited by executing a differing ratio of left and right turns ($\omega > \pm 500$ deg s^{-1}), and changing their mean heading angle back toward the plume, within the first second of leaving the plume. Comparing behaviors in and outside of the plume boundary reveal that mosquitoes increase crosswind velocities when outside of the plume, and accelerate upwind when inside the plume. We found that the difference in plume statistics, such as mean temperature, resulted in a difference in spatial distribution of the trajectories, suggesting that mosquitoes not only bias their trajectories toward the plume, but also to features of the plume.

Introduction

The hematophageous female mosquito requires blood proteins to fully develop eggs. Mosquitoes acquire these blood meals by detecting spatially and temporally complex windborne signals as they navigate to their host prey (Brown, 1966). Mosquitoes use a multitude of sensory modalities including chemosensory pathways (Brown, 1966, Davis and Sokolove, 1976, Dekker et al., 2005), mechanosensation (Ghaniana, 2007), hygrosensation (Rowley and Graham, 1968), and thermosensation (Peterson and Brown, 1951, Davis and Sokolove, 1975). Many behavioral investigations of host-seeking focused on the mosquito's robust response to CO_2 and other odors, such as lactic acid (Davis and Sokolove, 1976. However, mosquitoes are also attracted to warm surfaces (Maekawa et al., 2011, Spitzen et al., 2013, McMeniman et al., 2014), and can detect small changes in temperature (Gingl et al., 2005). Minimizing vector-host interaction is achieved by exploiting a deep understanding of how the vector navigates toward its host-prey. Thus, to understand mechanisms giving rise to spatial and temporal patterns of heat in which mosquitoes navigate, one must understand the physical nature of thermal energy transport in natural environments.

Three mechanisms govern the transport of thermal energy from a host (see for example Cambell, 1977): *conduction* - the transfer of thermal energy between juxtaposed matter, *convection* - the transfer of thermal energy through the movement of fluids, and *radiation* - the transfer of thermal energy through

massless particles (photons). Each of these three mechanisms contributes to vastly different spatial and temporal temperature patterns in natural environments. Radiative heat exchange, for example, follows from the movement of excited photons and behaves, therefore, independent of movement of surrounding, massed particles. As such, the spatiotemporal patterns of temperature depend on a mosquito's thermal perception of a host. The signal strength depends on the size (area) of the host and fourth power of host temperature. Moreover, radiative energy declines inversely with the square of the distance from the host.

An organism may also detect heat conductively, though only through physical contact with the relevant surface. Thus conduction, in the case of mosquito host localization, is only relevant in the moment a mosquito lands on the heater, or flies through the air immediately adjacent to the host.

The air heated by the host surface can be transported away via fluid motion. That transport, in turn, is a result of externally driven flows (forced convection) or flows induced by temperature-dependent buoyant forces (natural convection). In both cases, heat transport occurs in spatially and temporally complex plumes that flow through environments.

These vastly different physical mechanisms of heat transport lead to vastly different spatial and temporal patters of temperature cues in the environment. Thus the way in which mosquitoes detect thermal cues, and respond accordingly, depends on the type of thermal energy they are able to detect.

Gingl et al. (2005) showed that the thermosensors in *Ae. aegypti* – located at the distal end of the antennae – respond to changes in temperature, and are sensitive to rates of change in temperature as small as 0.002 C s^{-1}. The authors presented the sensilla with radiative and convective thermal stimuli, and found that mosquitoes have a lower convective:radiative ratio of response than some radiative-sensitive insects, e.g., the American cockroach (*Locusta migratoria*), and the locust (*Ixodes ricinus*). The authors claim this phenomenon results from the physiology and morphology of the sensilla, which differs from that of other thermonavigating insects.

Thermosensory structures are described as sensilla coeloconica, or peg-in-pit, and feature bowl-like cavity (pit) with a protrusion from the base of the bowl (peg) (McIver, 1973). The insects with peg-in-pit thermosensors, such as fire beetles, are generally known to thermonavigate via the detection of radiative signals (Schmitz et al., 2008). In the thermosensors of *Ae. aegypti*, the peg protrudes in close proximity to the walls, leaving only the tip of the peg exposed to interact with the air. Gingl et al. (2005) suggest that this morphological feature reduces the surface area with which mosquitoes can detect radiative energy. Further, radiative signals decay exponentially with distance. Given a warm blackbody (fully radiative, $\varepsilon = 1$) source at varying temperatures, detectable levels of radiative energy are only present centimeters from the source. While *Ae. aegypti* can possibly detect radiative energy, the probability of detection largely depends on distance, making it a highly improbable cue for navigation at large distances (> 1 m).

Previous studies of thermonavigation in mosquitoes did disambiguate the mechanisms of heat transport in providing cues for behavioral responses to thermal energy. Peterson and Brown (1951) showed that mosquitoes thermotax, and further showed that a difference in radiative emissivity did not have a significant effect on attraction, measured by landing frequency. The authors did not, however, examine flight behavior. In other studies, when a heated surface is presented, the type of thermal stimulus is not controlled, so both radiative and convective heat transport may occur (Lacey and Cardé, 2010), Maekawa et al., 2012, McMeniman et al., 2014). Thus, despite clear evidence of attraction to heat, it remains unclear whether how mosquitoes detect and navigate using convective thermal plumes.

This study seeks to determine whether the yellow fever mosquito, *Aedes aegypti*, exhibits behavioral responses in the presence of a thermal plume. To test whether mosquitoes can navigate to a host using convectively transported heat, I presented a thermal plume using gold-covered heated rods placed in a wind tunnel, and recorded the trajectories of freely flying, naïve, adult female mosquitoes. Polished gold has an exceedingly low thermal emissivity ($\varepsilon < 0.04$). With gold, or gold-covered thermal sources, the only thermal signals available to the animal were transported, rather than radiatively. Here, I present the first investigation of mosquito tracking behavior, in response to isolated convective thermal signal.

Methods

Animal husbandry

Yellow fever mosquitoes (*Aedes aegypti*) were housed communally (University of Washington, Seattle) under L:D cycle of 12h:12h, with temperatures between 26.3 - 27.3°C and relative humidity between 40 -52%. Mosquitoes had free access to a cotton ball soaked in 10% sucrose solution (Sigma Aldrich). Breeding mosquitoes in the colony were blood fed cow's blood (Sigma Aldrich) 5 times a week. Larvae and pupae were kept in plastic trays filled with MilliQ water (Sigma Aldrich) and fed newborn fish food (Hikari, First Bites). Male and female pupae were moved to two-compartment enclosures, and separated for experiments prior to eclosion.

Experimental animals were 4-14 day-old females, assumed to be mated, and not blood fed. 17 ± 5 mosquitoes were transferred at a time into a holding cage 0.5 h to 2 h prior to experiments, and were adapted, in the dark, to room conditions for at least 20 minutes before flights begun. Behavioral flight experiments were conducted in the last 2 h of photophase. Mosquitoes were used once per experimental condition. To minimize transfer of odorous skin oils onto surfaces, the holding cages were handled with gloved hands.

Wind Tunnel

All experiments were carried out in a 1 m x 0.25 m x 0.25 m (length x width x height) working section of wind tunnel (Figure 3.1A) with mean wind speed of 0.5 ± 0.1 m s^{-1}. The wind tunnel was constructed from transparent Plexiglas, with 0.56 m intake with 0.43 m length contraction section. Air was propelled through the wind tunnel from the containing room, using a blade fan (Dayton, model 2C363) and two aluminum honeycomb baffles (HoneyCommCore, ¼ inch cells) to reduce turbulence and entrance effects. Another baffle was placed at the downwind end, to suppress back-propagation of airflow induced by the fan. The airflow (0.5 ± 0.05 m s^{-1}, 26-29 C, 30-50% RH) was even throughout the wind tunnel except for a small boundary layer (~2.5 cm from the walls), with lowest wind speeds (0.29 m s^{-1}) measured just upwind of the heating elements. Air was exhausted into the containing room.

Experiments were conducted in dim light (0.3 ± 1 lux), provided by a string of cool white LEDs arranged beneath the working section. Two panels of infrared and visible (cool white) LEDs were placed below the working section. To diffuse light, we lined the exterior bottom of the working section with vellum. Checker patterned panels were placed on the outside of the length of the working section to provide visual stimuli. The pattern consisted of 12.7 mm squares of uniformly random grayscale shades. The walls of the working section were lined with corrugated cardboard to help maintain constant temperatures.

Mosquitoes were acclimated in the wind tunnel for at least 10 minutes, in the holding cage located on the midline, 9.8 cm from the floor, and 8.5 cm downwind from the intake screen. The holding cage constructed of a 3D printed frame, 7.62 cm x 7.62 cm x 10.6 cm (depth x width x height) in size. The walls of the holder were made of a fine mesh, with a sliding door that opened toward the floor. To minimize exposure to carbon dioxide and other human chemical cues during the experiment, the door of the holder was remotely opened using a motor outside of the wind tunnel. The cage was opened once during the recording session, and mosquitoes were allowed to freely fly out of the holder and throughout the wind tunnel. The surfaces in the working section of the wind tunnel were wiped down with 70% ethanol after each day of trials. A schematic of the working section is illustrated in Figure 3.1.

Video

To capture flight trajectories, we recorded mosquito flights using two infrared-sensitive, high speed cameras (Basler Scout A640, computar M0814-MP2 2/3" Fixed Lens, 8 mm) placed next to the working section, with a mirror placed above the working section, such that the plan view of the wind tunnel was captured from separate angles. The two cameras had overlapping views to allow 3D trajectory measurements. Videos were synchronously captured at 100 frames s^{-1}. Trajectories were digitized *post*

hoc using customized MATLAB scripts, and DLT data viewer (Hendrick, 2008). Cameras were calibrated by measuring locations of features on a custom-designed calibration object placed throughout the working section volume.

Thermal Plume Production

Three test conditions were used to compare search behavior:

Table 1 - Behavioral Test Conditions

Test Condition	**Stimulus description**	**Number of individuals**	**Number of trajectories**
Control	Clean air flow, heaters present and off	25	49
Left plume	Clean air flow, left heater held at 50 C, right heater present and off	28	52
Right plume	Clean air flow, right heater held at 50 C, left heater present and off	23	52

A thermal plume was produced by heating one of two steel cartridge heaters (Heatcon, 0.64 cm x 7.62 cm, with embedded type J thermocouple) located 0.15 m downwind from the intake screen. Each heater was placed 0.762 m from each side wall. The heaters were mounted in 3D printed airfoil holders, which placed the heaters 3.81 cm from the floor of the tunnel. We used a heater made from low-radiative emissive alloy ($\varepsilon = 0.2$). The heaters were coated in several layers of gold leaf (L.A. Gold 24 Karat loose gold leaf) to further reduce radiative emissivity ($\text{Ɛ} = 0.125 \pm 0.025$). We measured emissivity using an infrared camera (FLIR AS325sc), and the emissivities were measured using proprietary infrared measuring software (FLIR ExaminIR). Heater temperatures were maintained at 50.0 ± 0.1 C using a PID controller (Watlow EZ-ZONE PM Express). Surface temperatures of the heaters measured (33.7, 36.6 °C), and air temperatures in the wind tunnel with temperatures, with peak temperatures measured 2.0 cm from the heater (Figure 3.1B). One heater was powered at a time to produce convective plumes in a lateral location in the wind tunnel.

Plume Model

To characterize potential interactions of mosquito and thermal signal, a good estimation of the thermal dynamics must be made. The shedding of vortices from the heater and the buoyant forces produced by heat, in combination with the crossflow of the wind tunnel, allows predictability of gross features of the plume, such as elevation rate and crosswind radius. A mathematical model of plume shape

was calculated by implementing predictions described by Huq and Stewart (1996) and Prateek et al. (2012). Temporal statistics of temperature vary with distance from the plume boundary. For example, higher standard deviations of temperature were found near the theoretical plume boundaries (Figure 3.1C). Features like these were used to confirm the model (described in Chapter II). Plume boundaries used for behavioral analysis were defined by the model and were found to coincide nicely with expectations of edge, center and out of plume behavior (Figure 3.1D).

Trajectories

Digitized mosquito trajectories were processed such that small gaps (< 500 ms) were interpolated by a 3D cubic spline, and then passed through a linear Kalman filter, implemented with custom scripts (filtering matrix size to smoothing matrix size ratio 9:3). The trajectories were mapped with the dimensions of the wind tunnel.

If an individual mosquito flew out of the view of both cameras and then returned into view, the flight was counted as a new flight. If multiple individuals flew simultaneously in the wind tunnel, a mosquito leaving the frame could not be identified as the same individual with certainty. Thus, separating trajectories by off-screen occurrences minimized identification error, and estimation errors in interpolation.

Coordinates of the trajectories are in reference to a Euclidean origin, placed at the midpoint of the downwind edge at the floor of the working section of the wind tunnel, with the x as positive upwind, the y as crosswind, where positive values are rightward, and the z as positive , where positive values are upward (Figure 3.1).

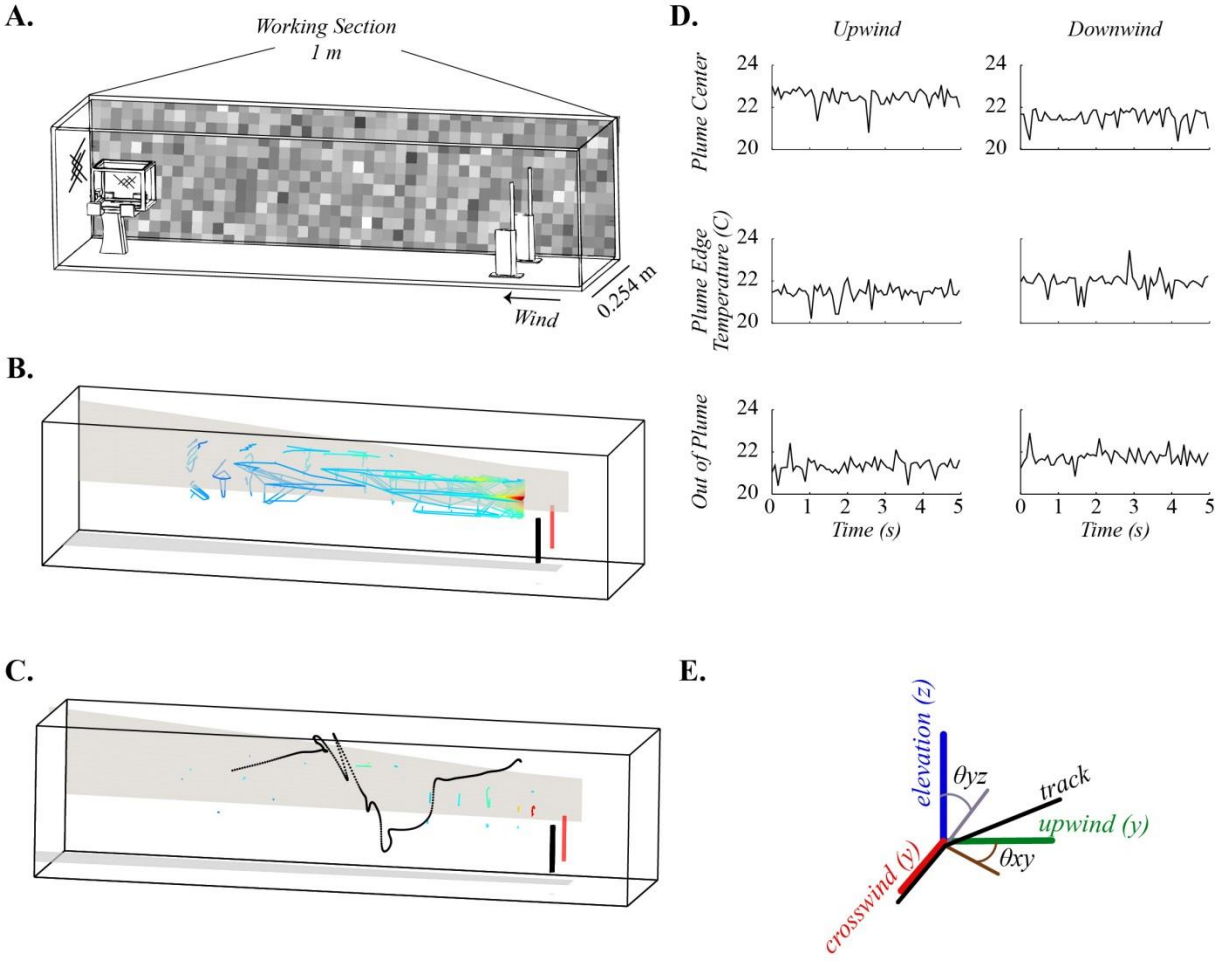

Figure 3.1 – Experimental setup and measurements. **A)** Schematic of working section of wind tunnel. The mosquito holder is located downwind, and heaters were placed upwind, atop airfoil-shaped holders. The outside of the tunnel were lined with a randomized grayscale box pattern to provide optic flow. **B**). Contour representation of time-averaged temperature measurements of the plume, within predicted plume bounds (gray projections). The heater locations are represented as black (non-warmed) and red (warmed) cylinders. Warm colors indicate warm temperatures. **C**) An example trajectory through the plume. Red points indicate positions within plume bounds. **D**) Time-varying samples of temperature at center, edge and outside plume locations. Variance is low in the center of the plume and outside the plume, and high at the edge. Center plume temperatures have a warmer average temperature. Downwind temperatures are cooler than upwind. **E**) Name and color scheme of wind tunnel dimensions, and how angular differentials are calculated.

Behavioral Analysis - Bootstrapping

To compare upwind positional distributions, we used the spatial distribution of positions from control flights to produce a prior for a boostrap from which we inferred statistical significance. We created a bias measure, and compared the bias measures between experimental and bootstrapped distributions. The bias measure is the proportion of points along the trajectories found in the left, upwind quadrant of the wind tunnel. This provides a single bias measure per experimental condition, and represents a probability measure of the experimental upwind distributions being drawn from the upwind control distribution.

Individual points were drawn from the trajectory ensemble from the control condition. Points were drawn, with replacement, such that the number of points equaled that of the test condition. A new distribution was recreated from these drawn points, and a bias measure was calculated. The drawing was repeated 1,000 times, and a probability distribution of bias values was calculated. The empirical bias measure for each test condition was compared to the corresponding bootstrapped distribution of bias measures.

This sampling strategy allows comparison of probabilities under the assumption that all locations are independent; however, positions along trajectories are temporally and spatially correlated, and thus are not truly random. To ensure that the correlation seen along a trajectory did not influence the bias or distribution seen, we carried out the same bootstrap procedure with entire trajectories drawn, instead of individual points. We found the resulting bias distributions to be sufficiently similar, and only use the independent point draw for analysis.

The distribution of biases was well-fit by a Gaussian, which, in assuming the observed mean and standard deviation are close or equal to the expected mean and standard deviation, can determine statistical significance of the observed left side bias. To test for significance, p-values were calculated manually, using the cumulative distribution function of the bootstrapped distribution. The value of the cumulative distribution function at the location of the empirical bias determines the p-value, and conventional 0.05 threshold was used as a determinant of significance. One-tailed tests were used; a right-tailed test was used for the right plume conditions, and a left-tailed test was used for the left plume condition.

Behavioral Analysis - Bioassasys

Position and derivatives of position were calculated from the Kalman filter. Instantaneous ground speed was calculated from velocities; however, instantaneous air speed could not be calculated due to the turbulent nature of the plumes. Additional kinematic parameters included angular velocity, and heading angle. Angular velocities are two dimensional, either in the horizontal (x,y) plane or the vertical (x,z) plane. Heading angle was considered only in the horizontal plane, and refers to the angular displacement

relative to the midline of the horizontal plane of the wind tunnel, with the upwind orientation equal to 0 degrees (Figure 3.1E).

Statistical comparisons typically require a normal distribution. Normality of kinematic distributions of the kinematics was analyzed by a Shapiro-Wilk normality test. The positional data was organized into regions of the wind tunnel (e.g. downwind, upwind halves) to test for large-scale changes in trajectories. Distributions of the kinematics were compared across regions and test groups were analyzed by a two-tailed Student's t-test, or, for non-Gaussian distributions, a simple sign test.

Angular velocity was used to define turn events in the flights. The angular velocity was well-fit by a sum of two Gaussians, and turns were approximated by thresholding absolute values greater than the standard deviations of the wider of the two fitted Gaussians. We defined a turn to be at least three consecutive time steps (0.03 s) above threshold. Left and right turns were determined by sign.

In-Plume and Out-of-Plume Behaviors

Trajectories were sectioned into in- and out-of-plume groups, based on boundaries determined by the plume model. The kinematics of these groups were analyzed by one-way ANOVA. Plume triggered averages were created by aligning kinematics by the moment the mosquito left the plume. Kinematics were averaged over 500 ms after the plume-leaving event and compared across conditions. To compare plume triggered averages of heading angles, the averages were binned into 500 ms segments and mean statistics were compared. Whether the distribution has a mean and differences in means across test groups were calculated by the Watson-Williams test. Comparisons were made in the full length of the wind tunnel and the upwind half of the wind tunnel.

Results

Distributions of Kinematics by Wind Tunnel Region

The distributions of mosquitoes along the crosswind and elevation dimensions varied significantly along the full length of the wind tunnel (Figure 3.2A). Crosswind distributions of only upwind positions (x > 0.5 m) showed a bias toward the side of the thermal plume (Figure 3.2B). Comparing the proportion of points found in one half of the plume to the bootstrapped probability function of bias values showed that the biases observed in the test conditions differed significantly from the mean (Figure 3, $p < 0.01$). Signed sample tests on the distributions also showed significant differences ($p < 0.05$). These data show that mosquitoes exhibit a biased crosswind behavior toward the location of a thermal plume. No other distributions of position varied significantly, suggesting behavioral decisions drive a difference in crosswind location.

Distributions of angular velocity in two planes (horizontal, w_{xy} and vertical, w_{yz}) were compared across upwind/downwind halves of the wind tunnel and all test conditions (Figure 3.3). No significant changes were seen in the distributions; however, there were significant differences in turn data derived from horizontal angular velocity. The mean number of total turns is significantly lower when the plume is present than when the plume is absent (one-way ANOVA, $p < 0.05$). The mean number of left and right turns that occurred in the absence of the plume was not significantly diffrerent; however, the number of left and right turns significantly varied when the plume was present. More right turns were made when the left plume was present and more left turns were made when the right plume was present (one-way ANOVA, $p < 0.05$, both conditions).

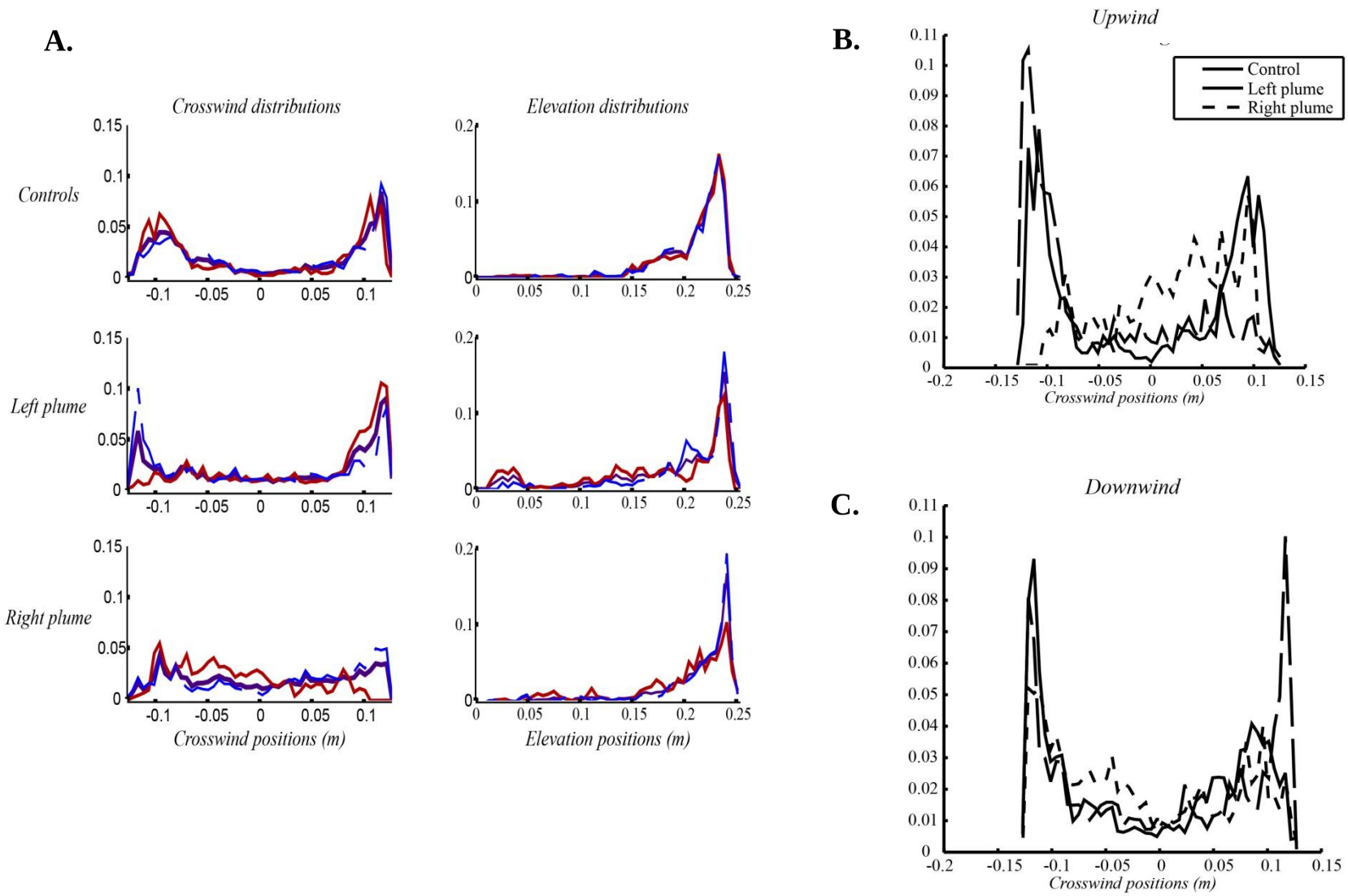

Figure 3.2 - Distributions of trajectory positions. **A**) Probability distributions of crosswind (left) and elevation (right) trajectory positions across test conditions for full wind tunnel length. No plume is shown in purple, left plume in blue and right plume in red. No significant differences are seen. **B**) Crosswind distributions measured in the upwind half of the wind tunnel. No plume is plotted with a solid line, right plume with a short dash line and left plume with a long dash line. Not the trend toward the heated side in the plume conditions. **C**) Crosswind distributions measured in the downwind half of the wind tunnel.

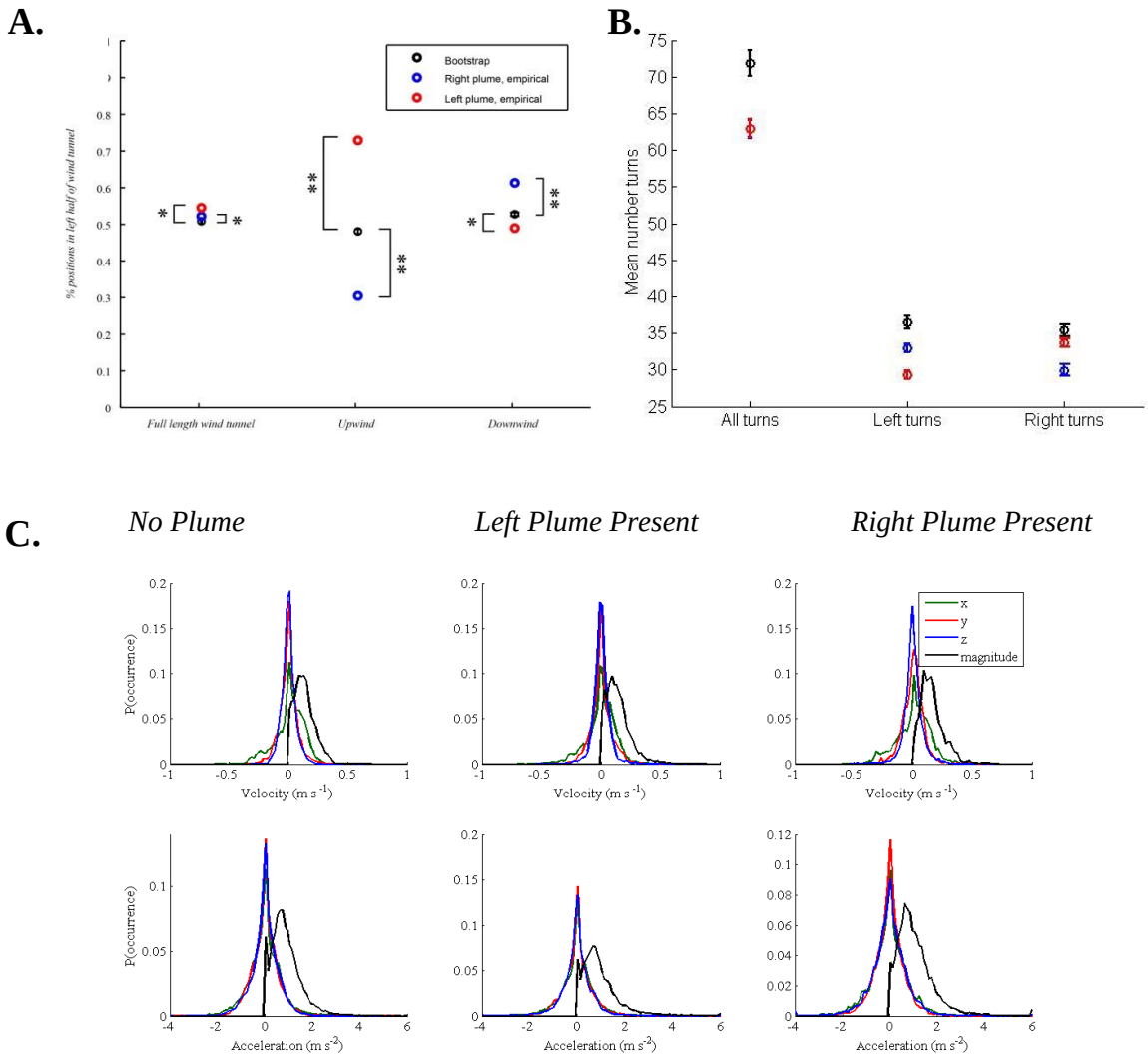

Figure 3.3 - Observed kinematics of flight. **A**) Bootstrapping and empirical side biases. The means and standard deviations of the probability distributions for the bias values are plotted by condition and wind tunnel segment. A single asterisk (*) denotes $p < 0.01$, while a double asterisk (**) denotes $p < 0.01$. Black denotes control condition, blue denotes that right plume present and red denotes that left plume present **B**.) The mean number of turns is plotted for each condition. **C**) The distributions of velocity (top) and acceleration (bottom) across test conditions.

Kinematics In vs. Out of Plume

The mean percent time spent in the plume boundaries varied significantly with presence and position of the plumes ($p << 0.01$, two-way ANOVA). However, no clear trend seen to describe how trajectories changed with plume position or presence (Figure 3.4A).

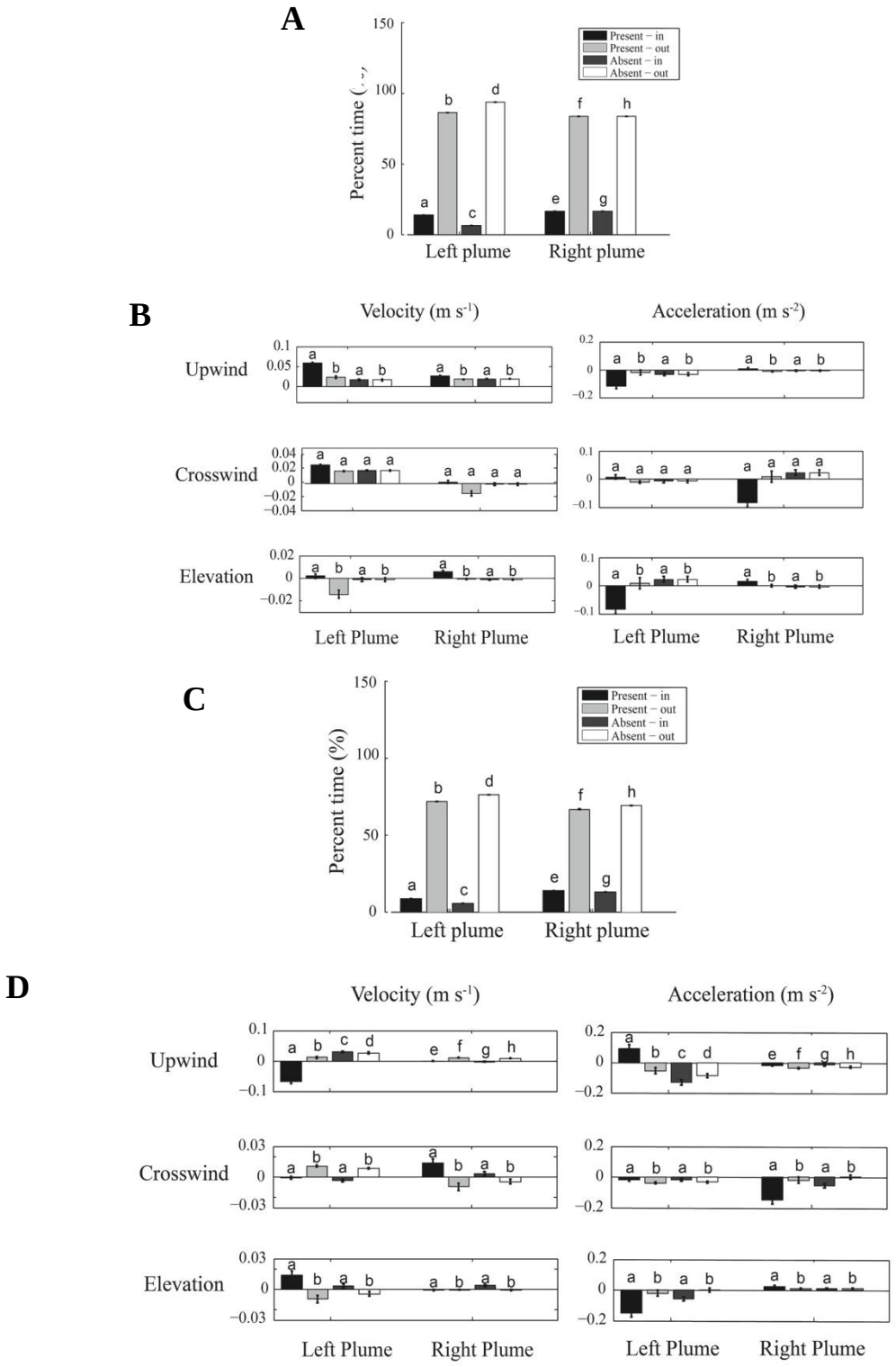

Figure 3.4 – Kinematics in and out of plume boundaries. **A**) Average time spent in plume per trajectory, for the full length of the wind tunnel. Behaviors are grouped according to plume position (left, right) and presence. **B**.) Mean velocity and acceleration for positions along the length of the wind tunnel in each dimension of the wind tunnel. **C.**) Mean percentage time in plume and **D**) mean velocity and acceleration in upwind half of the wind tunnel. Letters denote groups of differing statistical significance. Error bars are standard error.

Figure 3.4 (B and C) show variation in velocity and acceleration relative to the plume presence and position. For the full length of the wind tunnel, upwind and elevation velocities and accelerations differed across plume positions, but not presence (p <0.01, p = 0.24, respectively). For all conditions, there was a mean upwind (x) velocity. Crosswind (y) velocities were, on average, rightward with the left plume present, and leftward for the right plume present, were not significantly different. Elevation (z) velocity varied with no obvious trend, although position did vary significantly ($p<0.01$). Accelerations followed the velocities inversely, suggesting that a gradual slowing occurred.

In the upwind half of the wind tunnel, upwind velocity varied with plume presence and position together. There was an average negative—or downwind—velocity seen within the left plume position, while the average velocity in the right plume was near zero. The crosswind and elevation velocities and accelerations varied by position, but not presence. Upwind accelerations in the upwind half were again the inverse of the velocities, here denoting a trend of gradual acceleration with the general upwind progress of the trajectories.

Heading angle distributions of the full length of the wind tunnel were dominated by up- and downwind directions (Figure 3.5A). In the upwind half of the wind tunnel, with no plume present, there was a slight rightward bias in the heading angles. With the plumes present, the mean heading angle had a bias toward the side opposite of the plume position (Figure 3.5A).

Plume triggered kinematic distributions of heading angles, in the second two 0.5 s bins, a gradual oscillation in mean heading angle was seen (Figure 3.5B). With the left plume, in the first bin, the mean heading angle was in the direction of the plume. That is, the mean medial exit heading angle was leftward, while the mean lateral exit heading angle was rightward. In the following two time periods, the mean heading angle was toward the plume, and then away from the plume in the final time bin. A similar pattern was seen for the right plume, except that in the final time bin, the heading angle was nearly upwind. These slow oscillatory behaviors were similar to when the plume is absent, but the plume-present headings tended to be more upwind.

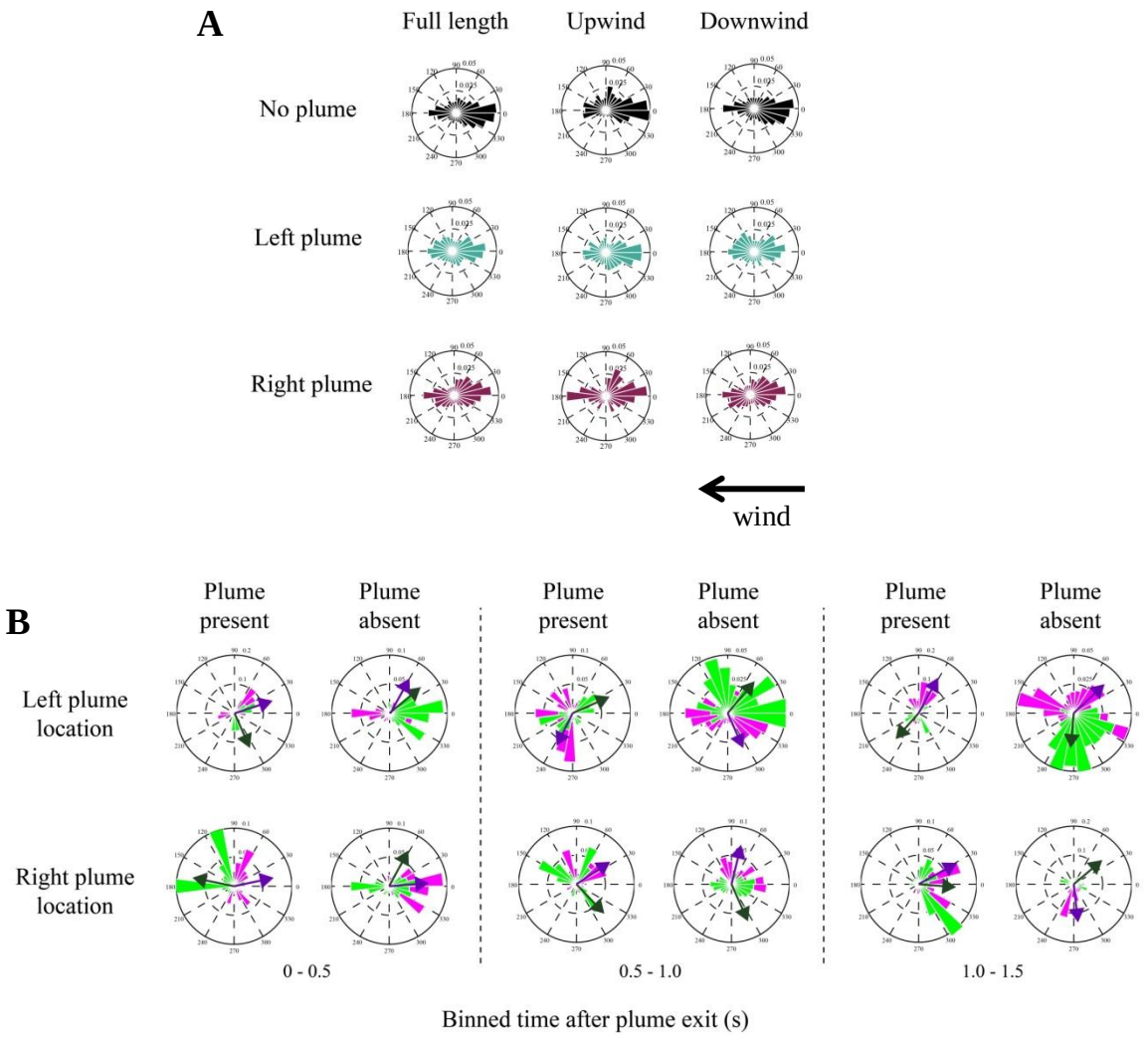

Figure 3.5 – Heading angle distributions throughout wind tunnel volume. A) Distribution of heading angles in various segments of the wind tunnel, for each test condition. Upwind distributions, with the plumes present, have a slight bias in the opposite direction than the plume positon. With the plumes absent, there is a slight rightward bias in the distribution. B) Distributions of heading angles seen after the mosquito exits the plume (plume-triggered average), binned over sequential 0.5 s intervals. Distributions are divided into medial-headed direction (purple) and lateral-headed directions (green). Oscillation in mean heading angle is seen when the plume is present such that the mosquito either flies downwind back into the plume (left plume) or narrows its heading to be more upwind (right plume). Mean heading angle is indicated by arrows.

Discussion

We found that female mosquitoes exhibit a position bias in response to the presence of a convective thermal plume, with minimized radiative signal. The mechanisms that drive this overall bias were not readily evident in differences in kinematic distributions (Figure 3.3), and typical plume navigation

behaviors, such as casting and surging were not seen. After careful exploration of the data, we found evidence for behaviors driving convective thermonavigation.

Three comparisons can made from the data: 1) differences among plume presence—differences in this comparison indicates the effect of plume presence on trajectories, 2) plume position (left or right)—differences here indicate the effect of space, e.g., proximity to the wall or boundary layer of the flow, and 3) plume position and presence—differences here would indicate the combined effect of the plume and location on flight or that the plume feature changes as a function of position.

The percent time spent in the plume had significant differences of this third nature (Figure 34A). Without clear in plume position or presence, so it remains unclear how the plume or spatial components influence mosquito flight. It is likely that the plume boundaries do not have a robust effect on flight. For example, if the plume navigation strategy requires a crossing of the plume, but not attempts to remain within the plume bounds, then samples will be small (resulting in a low percent time in plume as we have observed), and the behavior with each crossing may vary, resulting in erratic and dynamic statistics. Dekker et al. (2005) observed that mosquitoes did not spend much time within the plume boundaries, when they were presented a laminar CO_2 plume.

The majority of the plume-related responses were seen in the upwind (x) direction. More downwind-directed flight was seen with the left plume but not the right. Absolute velocity was found to be significantly greater outside of the left plume than inside the left plume; however, this trend was not seen for the right plume or with plumes absent.

From our observations, we found that there are features of mosquito flight that vary with position in the wind tunnel and presence of the plume. Crosswind and elevation velocities and accelerations varied significantly with position in the wind tunnel. From this we can determine that the difference in velocity and acceleration in the crosswind and elevation dimensions are dictated by position in the plume. This follows logic, as the mosquitoes spend most of their time near walls and the ceiling. There were no differences in effect with upwind flight or upwind half of the wind tunnel. These data suggest that behaviors were seemingly obscured or dominated by the more salient response to proximity to walls and ceilings, respectively.

Thermonavigation has often been considered a modality that works in concert or complement with other modalities (Lacey and Cardé, 2010, Maekawa et al., 2012, McMeniman et al., 2014, van Breugel et al., 2015). Furthermore, the specification of thermal stimulus has rarely been made, so studies that do consider thermosensitive responses usually include a mixture of thermal and radiative energies. While this is beneficial to understanding general host-seeking behavior, it precludes knowledge of how windborne

thermonavigation is accomplished. We show, for the first time, that *Aedes aegypti* bias their flights toward the location of strictly convective thermal plumes.

We found that the mosquitoes spend more time in the crosswind (left or right) half of the wind tunnel containing the plume when the plume is present. There is also a decrease in the total number of turns, with an increase in turns toward the side opposite to the plume position. The mean heading angles, in the presence of the left and right plumes, were approximately -20 degrees and -5 degrees, respectively. Outside of the left and right plumes, the average heading angle was 15 degrees and -10 degrees, respectively, indicating that the trajectories, on average, were slightly biased to the left. If a mosquito were aiming to remain within or near the plume, leftward turns would correct the rightward bias. The inverse is true in the case of the right plume; however the bias is much slighter. Initially, this result seems counterintuitive; however, the binned heading angle distributions help to clarify this confound. The slow oscillation of mean heading angle shows that the mosquitoes head away from the plume before returning toward the plume (Figure 3.5B). The direction of turns is dependent on the track, so when the mosquito has a mean heading angle toward the center of the wind tunnel (medial-exit), a left turn or series of left turns will return the mosquito to the right plume, and vice versa. Thus, the confounding disparity in turning ratio can be explained by turning back toward the plume location, given how they exit the plume.

It is important to note the difference between left and right behaviors. First, the overall spatial distribution of mosquitoes with the left plume present is qualitatively similar to that of the control (Figure 3.5). This disparity is echoed in the kinematics of the left and right plumes, as is clearly illustrated in Figure 3.4. The difference seen is likely driven by the difference in plume temperature and structure seen in our experiments. The heating rod surface temperatures differed by 2.9 C. The difference in source and ambient temperature influences height, spread and turbulence of the plume. Thus, the left plume was found to be less turbulent, less buoyant and containing temperatures closer to ambient, in comparison to the right plume. This difference in plume features may explain the differences seen in the kinematics, such as downwind velocities seen in left plume boundary when the left plume is on (Figure 3.4C). The difference in plume boundaries also influences statistical measurements, as more of the area of the wind tunnel is considered. Spatial influences on the trajectories may thus obscure influences plume presence can have on flight.

We saw that, with the plumes present, mosquitoes fly upwind when outside of the plume, and exhibit faster upwind accelerations within the plume. Crosswind flight is close to zero within the plumes. While no clear casting and surging patterns were qualitatively identified, the observed behavior is in line with typical features of plume tracking, wherein exploitative (here, upwind) flight is seen in regions of large information, and explorative (crosswind flight) is seen when signals are sparse or uninformative.

Interestingly, no changes in kinematics corresponding to elevation were seen. The plume is expected to be turbulent, with much of the mixing occurring above and below the plume center (Hoult and Weil, 1972). This behavior is at least partially explained by the lateral nature of the stimulus. With vertical mixing occurring, the larger changes in temperature and other plume stimuli will occur in the crosswind dimension.

We can therefore conclude the mosquitoes adjust their turning ratio, upwind and crosswind velocity and accelerations, but not height when navigating our thermal plumes. The superficial biases seen in all behaviors are still very slight, and, as seen in similar research, the kinematics are noisy. It may be that flight is intrinsically noisy for a strategic reason, e.g. to increase chances of coming in contact with host cues. Alternatively, thermonavigation alone may not strongly influence flight patterns. Thermal signals and other sensory modalities have been found to interplay to improve search efficiency. Multimodal interactions have shown that the presence of one signal modality may increase the sensitivity to others. For example, the presence of carbon dioxide increases sensitivity of detection of lactic acid and temperature (McMeniman et al., 2014) and to visual cues (van Breugel et al., 2015). It is therefore important to consider how these sensory systems work independently, to gain clearer insight into how these modalities may be enhanced, either through neural mechanisms or behavioral strategies, when combined.

Our findings suggest that mosquitoes are capable of tracking thermal plumes, and the temperature and structure of the plume correlate with the behavior. When plume tracking experiments include a heated source of any sort, one should consider the effect of thermal energies on the plume as well as the tracking behavior. Further exploration of thermal plume interactions can be determined using computational models, exploring the crosswind and upwind interactions between the plume and flight dynamics.

References

van Breugel, F., Riffell, J., Fairhall, A., & Dickinson, M. H. (2015). Mosquitoes Use Vision to Associate Odor Plumes with Thermal Targets. *Current Biology*.

Brown, A. W. (1966). The attraction of mosquitoes to hosts. *JAMA*, *196*(3), 249-252.

Campbell, G.S. (1977. Attenuation of Radiation. *An Introduction to Environmental Biophysics*. Heidelberg Science. 157.

Davis EE, Sokolove PG. (1975). Lactic Acid-sensitive receptors on the antennae of the mosquito, *Aedes aegypti*. *Journal of Comparative Physiology A*. **105**:43-54.

Davis EE, Sokolove PG. (1976). Temperature responses of antennal receptors of the mosquito, Aedes aegypti. *Journal of Comparative Physiology A*. **96**:223-236.

Dekker T, Cardé R. (2011). Moment-to-moment flight manoeuvres of the female yellow fever mosquito (Aedes aegypti L.) in response to plumes of carbon dioxide and human skin odour. *Journal of Experimental Biology*. **214**.

Dekker T, Geier M, Cardé RT. (2005). Carbon dioxide instantly sensitizes female yellow fever mosquitos to human skin odours. *Journal of Experimental Biology*. **208**:2963-2972.

Gingl E, Hinterwirth A, Tichy H. (2005). Sensory representation of temperature in mosquito warm and cold cells. *Journal of Neurophysiology*. **94**.

Lacey ES, Cardé RT. (2010). Activation, orientation and landing of female Culex quinquefasciatus in response to carbon dioxide and odour from human feet: 3-D flight analysis in a wind tunnel. *Medical and Veterinary Entomology*. **25**.

Maekawa E, Aonuma H, Nelson B, Yoshimura A, Tokunaga F, Fukumoto S, Kanuka H. (2011). *Parasites and Vectors*. **4**:10.

McIver, S. B. (1973). Fine structure of antennal sensilla coeloconica of culicine mosquitoes. *Tissue and Cell*, *5*(1), 105-112.

McMeniman C, Corfas R, Matthews B, Ritchie S, Vosshall L. (2014). Multimodal integration of carbon dioxide and other sensory cues drives mosquito attraction to humans. *Cell*. **156**.

Schmitz, H., Schmitz, A., Kreiss, E., Gebhardt, M., & Gronenberg, W. (2008). Navigation to Forest Fires by Smoke and Infrared Reception: The Specialized Sensory Systems of "Fire-Loving" Beetles. *Navigation*, *55*(2), 137-145.

Spitzen, J., Spoor, C. W., Grieco, F., ter Braak, C., Beeuwkes, J., van Brugge, S. P., ... & Takken, W. (2013). A 3D analysis of flight behavior of Anopheles gambiae sensu stricto malaria mosquitoes in response to human odor and heat. *Tissue Cell* 5: 105–112.

Hedrick, T. L. (2008). Software techniques for two-and three-dimensional kinematic measurements of biological and biomimetic systems. *Bioinspiration & biomimetics*, *3*(3), 034001.

IV.

Modeling Behavioral Policy of Thermonavigation

Abstract

Mosquitoes navigate toward hosts following plumes of airborne cues emitted by their host-prey. Movement of host prey or obstacles in the environment often results in turbulent or intermittent plumes. The difficult task of tracking a meandering, turbulent plume to its source has been investigated mostly through investigation of moth olfactory detection and flight behavior. Olfactory search behaviors are often quantized into the search states of biased random walk, surging, and casting. These states typically correspond to plume finding, plume detection and plume recovery, respectively. In our work, we have investigated whether mosquitoes' thermotaxis toward convective thermal plumes is consistent with strategies of olfactory search. We find that while the mosquito is capable of biasing its location toward thermal plumes, these distinct behavioral states are not evident. Under our experimental paradigm, mosquito thermal search is characterized by highly variable heading angles (angle of trajectory relative to due-upwind direction). Other kinematics such as velocity and acceleration do not change significantly during plume tracking, despite large scale, significant biases in distribution of positions. Here, we present the preliminary formulation of a plume-seeking agent-based model that seeks to reproduce the behavioral strategies observed experimentally. Our goal is to evaluate possible ways in which the thermal stimulus may affect the mosquito's intrinsic flight patterns to generate the observed flight statistics. We describe mosquito search strategies using a dynamical model which is driven by a three-dimensional random force, and is biased by interaction with the wind, spatial boundaries, and the plume. This model serves as a platform with which free flight statistics can be reproduced, and information processing strategies for search efficiency can be tested.

Introduction

Navigating to the source of a convective signal is nontrivial as airborne stimuli are highly spatiotemporally dynamic and sparse. Mosquitoes are adept at accomplishing this task, and have been observed to detect and navigate plumes of carbon dioxide and lactic acid, among other windborne stimuli (Dekker, et al., 2005, Geier, et al., 1999). Thermal signals provide another windborne cue that a mosquito can use to navigate its environment (Brown 1951, Maekawa, et al., 2012, McMeniman, et al., 2014). We have shown that female *Aedes aegypti* mosquitoes indeed exhibit a bias toward the crosswind position of a convected thermal plume (Chapter III). However, we found few clear temperature-dependent changes in mean kinematics, and also did not observe discrete behavioral search patterns, such as casting and surging, that are typically seen in olfactory plume navigation. Rather, we found that mosquito flight kinematics have large variance. We observed uniform distributions of heading angles, suggesting that there are many changes in direction, speed, and rotation in a given trajectory. Here, we aim to characterize mosquito flight quantitatively and statistically and to develop a platform to test different models for how the animal may interact with the thermal plume.

Mosquitoes exhibit flight behaviors that are not commonly seen in Diptera, such as side-slipping, a lateral translation achieved by rolling without yawing (Iams, 2012). For any sensory-relevant movement,

the placement of the body affects the local environment and therefore stimulus the organism can detect. With side-slipping, a mosquito translate crosswind with the body axis of the mosquito remaining parallel to the flow, affecting how forces act on the body and available sensory features the mosquito is able to detect given its orientation. Features like side-slipping may exist as a way of making flight more efficient by minimizing drag forces, and may also help contribute to unique mosquito flight dynamics..

To approach elucidate mechanisms of convective thermal plume tracking, we created a dynamical agent model of a mosquito, wherein the agent's movement is modeled as a damped system driven by forces acting on a mass. Modeling the flight of a mosquito in this manner lets us not only to impose naturalistic, local environmental forces onto the agent, resulting in naturalistic features, such as delays in response and perturbations in the flight path, but also allows ready application of the model to robotic devices.

There are a variety of previous agent-based models for plume search. Behavioral models of plume search seek to reproduce the frequency and time in which it takes the organism to arrive at or near the plume source. Many of these models are based on moth behavior in response to pheromone plumes (Dusenbery 1997, Farrell et al., 2002, Belanger & Willis 1998, Grubaum & Willis 2015, Bau & Cardé 2015). Such models have been categorized as either *reactive* or *cognitive* (Bau & Cardé 2015). Reactive models are those which are constructed based on behaviors (described in Table 1) that are triggered in response to signal encounters, such as casting, spiraling, and surging (Martinez & Moraud, 2013). Cognitive models are those which reproduce search patterns based on encoding properties of the agent. These behaviors are often achieved by optimizing or refining a combined history of encounters and spatial knowledge. Examples of drivers of cognitive models include Bayesian inference, gradient descent or maximizing information (Huang, et al., 2010, Pang & Farrel, 2006, Bachmayer & Leonard, 2002, Vergassola et al., 2007).

Each of these modeling strategies of course has benefits and drawbacks. Reactive models are computationally minimal, and can easily be mapped to neurological processes and demands seen in insects . Reactive models are often constrained by characteristics of behavioral responses of the modeled organism, and may not result in naturalistic or efficient searches. Cognitive models can easily recreate characteristics and features of plume tracking behavior, and are excellent for deriving a plume following strategy that is applicable in a variety of environments. Cognitive models, however, may require more computational demand than an insect can feasibly produce.

Table 1 – Glossary of behavioral strategies.

Cast	Crosswind oscillation.
Surge	Bout of straight flight, typically upwind and of greater velocities.
Spiral	Flight that roughly follows an Archimedes spiral, growing in diameter over time.
Cast-surge	A combination of casting and surging wherein casting typically occurs when the signal is lost for some period of time or distance.
Spiral-surge	A combination of spiraling and surging wherein spiraling typically occurs when the signal is lost for some period of time or distance.

There are many examples of reactive models. Belanger and Willis' (1998) reactive model, based on moth behavior, the agent would head upwind (surge) if an odor was detected, perform crosswind oscillations (cast) if the odor was lost, and increase the oscillation amplitude over time. The model was optimized using a genetic algorithm and trained to increase the success rate (flying near the source). The authors found that two strategies—slow wide oscillations and fast narrow oscillations—were equally efficient. In this model, the wind direction was held constant. The authors proposed that changes in wind direction would encourage a different behavioral strategy.

Lochmatter and Martinoli (2009) expanded on the Belanger and Willis model, comparing performance of pure casting, spiral-surge and cast-surge strategies, while also testing whether wind direction detection affected performance. Here, the agent's behavior before interacting with the plume is characterized as a largely-upwind flight, held at a fixed angle relative to upwind. Plume loss is determined by the amount of distance traveled since the last detection event. In spiral-surge and cast-surge strategies, when the plume is lost, the agent either cast (head directly crosswind) or spiraled (Archimedes spiral) until the plume was contacted again. Any time the behavioral state changed, the wind direction was detected, either stochastically or deterministically. The authors considered the deterministic wind detection to be an ideal performance. The authors found pure casting to be an inefficient search, and local search behaviors, such as casting or spiraling, when the plume produced successful searches with variable signal types. The authors also noted that wind angle detection affected search performance, while the time or distance between plume encounters did not. Since the plume is stretched longitudinally as it is spread down wind, logic dictates that accurate tracking of wind direction lends to more efficient search than keeping track of the last-detected signal.

In a beautiful recent study of reactive plume search models (Bau and Cardé, 2015), the success of a number of strategies in response to plume finding and loss are compared. The authors described three types of navigational strategies: 1) biased random walks – movement with even step lengths and random

directions taken at each time step, plus constant movement in a singular direction, such as upwind or crosswind, 2) Lévy walk – movement with random direction and step lengths with a heavily tailed distribution, resulting in occasional surges, and 3) intermittent random walks – movement characterized similarly to biased random walks, where the bias movement is intermittently applied. Bau and Cardé compared the performance of these three strategies in virtual environments with varying wind direction fluctuation and number of plume sources. The authors found that intermittent random walks, Lévy walks, and random walks with an upwind bias produced the highest success rates in all wind regimes, while pure casting and pure upwind surges were inefficient. They also found that, after losing contact with a plume, strategies that employed local search, such as casting worked best. Similar to the Belanger and Willis model, the authors found increasing the width of oscillations over time, or having one large amplitude crosswind oscillation after a plume-loss event significantly increased plume reacquisition and success rates. This model factors in meandering of plume centerlines but does not consider intermittency, producing a model that describes a gross-scale plume tracking behavior.

Each of these models were two dimensional, as moth flight and pheromone plumes have little variance in the vertical dimension. Some features of flight, such as a mean upwind heading angle and spiraling when the plume was lost, are not behaviors often seen in moth flight. These models can reproduce features of the organismal performance for which they are modeled. However, they are not necessarily applicable to mosquito flight, which lack surging and casting behaviors in the presences of convective thermal plumes. Thus, a reactive model of mosquito search would have to employ a different set of dynamics and behavioral response.

Perhaps the most frequently discussed cognitive model of plume search is infotaxis (Vergassola et al., 2007). Vergassola et al. used Bayesian inference to maximize information gain. The agent model consisted of two gross states: exploration – the state in which the agent would gain as much information about its environment by building a probabilistic map, and exploitation – the state in which the agent moves toward the location with the highest probability of having the source. These states were both derived from the decision strategy that minimized entropy. At each time step, the agent would decide to move toward the position which minimized entropy, which included remaining in the same position. Interestingly, this strategy produced trajectories that had spiral-surge or cast-surge features.

The robustness of the infotaxis model lies in the ability to navigate toward a source despite a heterogeneous and meandering plume structure. In the initial implementation of infotaxis, the signal presences is treated as either a hit or a miss, with a Poisson distribution whose mean given by the average plume envelope at that location. Independent of this specific choice, it is assumed that the agent knows the distribution of cue occurrence. Mosquitoes are known to track plumes of various statistical structures, weakening the application of infotaxis to mosquito plume navigation. (The application of infotaxis can be

bolstered, however, if one assumes mosquitoes are able to develop Bayesian inferences about the statistics of the plume, as explored by Huang, et al. (2010).) While conceptually elegant, infotaxis is unfortunately computationally very demanding. Bau and Cardé (2015) suggest that the computational demands are outside the feasible realm of insect computation, including mosquitoes.

Our model exploits the advantages of both reactive and cognitive models. We have formulated an agent-based model, developed from observations of convective thermal plume tracking by female mosquitoes. The model is three dimensional, as convective thermal plumes (and possibly the behavioral response) have a pronounced vertical rise. We use a plume-response-dependent directional bias shift, and history-dependent duration of directional bias, thus producing a model that possesses a combination of reactive and cognitive model features. Search performance was optimized by minimizing the differences in kinematic distributions of the agent and the behavioral data. Thus, the model will help test how slight reactive responses can lead to large-scale changes in behavior, as observed in our behavioral experiments. Ultimately, we aim to determine the behavioral policies of mosquito flight in response to position within the wind tunnel, and position of a turbulent thermal plume.

The model presented thus far explores advantages of this reactive-cognitive hybrid model structure. Further developments in the model, however, can include behavioral responses to statistics of the convective thermal plume, making it a robust and powerful tool with which one can 1) derive signal statistics that may be neurally encoded to make navigation decisions, and 2) determine a plausible decision policies based on corresponding behavioral changes. With this computational model, we will explore the closed system of sensory detection and behavior. By having specific control of the stimulus, and apply behavioral rules derived from experiments, we can simulate behavioral response to the stimulus.

Methods and Materials

Model algorithm

The agent is modelled as a point mass with mass *m* that moves in a volume with the same dimensions as the experimental wind tunnel's working section and with heat sources in the same locations. To capture the smoothness of real trajectories, we assume that the agent's movements are damped. Thus, Newton's law for the agent's movement gives

$$m\vec{\boldsymbol{v}} = -\eta\vec{\boldsymbol{v}} + F_{driving}, \tag{4.1}$$

where $\vec{\boldsymbol{v}}$ is the three-dimensional velocity, η is the damping coefficient. We also assume that the animal is subject to $F_{driving}$, a set of driving forces, which represent forces produced by the mosquito during flight.

We define the driving force as a weighted sum of postulated forces that model the motor and muscular output employed in mosquito flight along with environmental influences:

$$F_{driving} = aF_{baseline} + bF_{upwind} + cF_{repulsion} + dF_{stimulus}. \quad (4.2)$$

The dominant driver is the baseline force, $F_{baseline}$, which is a stochastic force whose direction is uniformly random in three dimensions. These random vectors were generated by first generating points that were uniformly distributed in all directions by drawing from a three-dimensional Gaussian distribution. These points were then scaled to the unit sphere, producing unit vectors.

The unit vector magnitudes were then scaled to match magnitudes seen in the experimental data. We found the magnitude distribution was best fit by a log-normal function $\boldsymbol{N}(\ln x,\mu,\sigma^2)$. However, lognormal distributions have a very long tail, with non-zero probability of drawing an extremely high value. These rare draws result in behaviorally unrealistic instantaneous accelerations, thus the right tail of the force distribution was truncated to a maximum value of 3 x 10^{-4} N.

Table 2 –Distribution parameter values.

Function	Variable	Value
Log normal force magnitude	Mean, μ	0.60
Log normal force magnitude	Variance, σ^2	0.72
Log normal force magnitude	Amplitude, A	4.47e-6

To generate the upwind bias observed in mosquito flight, a constant upwind force vector, $F_{upwind} = \begin{bmatrix}1\\0\\0\end{bmatrix}$, is applied at each time step.

The mosquitoes do not distribute themselves uniformly throughout the wind tunnel volume; they tend to cluster with higher probabilities near the walls and ceiling, presumably in response to the wind conditions, such as boundary layer, and visual cues. To reproduce the baseline position distribution seen in control conditions, we derived a repulsion force, $F_{repulsion}$, from the experimental position distribution in order to bias agent movement toward the regions of high probability. The forces vary throughout the volume such that the direction and magnitude of the force is dependent on the agent's position at a given time. $F_{repulsion}$ is a constant force, applied in all three dimensions.

The $F_{repulsion}$ magnitude was drawn from fitted probability distributions of position. We found the crosswind, *x* distribution to be best fit by a linear regression, the upwind distribution, *y*, was best fit by a 6th order polynomial (r^2 = 0.959), and the elevation distribution, *z*, was best fit with a sum of three

Gaussians (r^2 = 0.995). The direction of $F_{repulsion}$ was the opposite sign of the derivatives of distribution functions in each dimension.

Flight simulations

When a flight is simulated, agents are instantiated with an initial position and velocity. The position is uniformly randomly drawn from a vertical plane at 0.1m, corresponding to the downwind boundary of the mosquito cage in experimental wind tunnel. Initial velocity is a random draw from a normal distribution, which is fitted to experimentally observations: ***N****(0, 0.01)*.

Note, that mass and damping has the physical interpretation the weight of the mosquito and the drag forces on the mosquito's body during flight. However, we assume the mosquitoes have a "behavioral" mass and damping. Here, we treat mass and damping as a combination of physical and behavioral characteristics.

Boundary interactions

The acceleration, velocity, and position are derived from the total forces produced at each time step. To enforce spatial boundaries, we checked whether the position at each time step was within the bounds of the virtual wind tunnel. If outside the bounds, the event is treated as if the agent has collided with the wall. That is, the direction in of the wall collision is made negative, sending the agent toward the center of the virtual wind tunnel. The corrected, in-bound position is used for a given time step.

Parameter Optimization

Agent movement is derived from a weighted sum of internal forces, as described in Eq 4.1. The agent's baseline behaviors were defined by changing the coefficients of each force, such as mass, *m*, and the damping coefficient, η. The mass and damping coefficients were considered a combination of real-world values and effective mass and damping produced by behavioral forces. The mass and damping coefficients were no less than the real world values or approximated values (mass = 2.88 g).

We optimized the model by an unbounded Nelder-Mead simplex algorithm, the cost function of which minimized the sum squared error (SSE) of the model output and the behavioral kinematic distributions (position, velocity, and acceleration). We used selected coefficients from Eq. 4.1 to optimize the model. We optimized the model to best match the velocity magnitude and acceleration magnitude distributions of the experimental data.

Baseline Behavior

Baseline agent behaviors were modeled on flight trajectories recorded during control sessions (with no heater on). We assume the occurrence of these behaviors as responses to non-thermal signals, such as low resistance in boundary layers or visual cues. When the plume is absent, $F_{stimulus} = 0$.

Stimulus Behavior

To examine the impact of the proposed behavioral policy on agent behavior, stimulus force was imposed conditionally. The convective thermal plume was represented as a volume in the shape and position of the experimental convective thermal. The plume shape was approximated by a model that described boundaries, as described in Chapter II. We instantiated the plume as a binary stimulus, and imposed the following biases based on the agent's interaction with the plume:

Condition	**Stimulus-bias Forces Applied**
Plume naïve	*Baseline forces only*
Entering plume	*Upwind bias increased*
Exiting plume, left	*Stimulus force - right bias*
Exiting plume, right	*Stimulus force - left bias*

The stimulus force is initially applied when the agent enters the plume, and persists until the plume is once again encountered. If the plume is not encountered again within 10 time steps, the agent condition returns to the plume naïve state.

Model testing

We tested whether directional biases of a random walk, enacted when the agent encounters a plume stimulus, can produce small changes in kinematics, and large changes in gross features, such as a shift in position distribution shift. To test this behavioral policy, we added the conditionally dynamic stimulus force, $F_{stimulus}$.

Each agent flight ended when either 1) the agent reaches the upwind wall, 2) the agent contacts the surface of the heater, or 3) allotted amount of time (15 s) is surpassed. For each test condition, we ran 200 model trajectories and calculated velocity and acceleration distributions for each dimension and magnitude. Accuracies of model outputs were compared to the behavioral data by the chi squared statistic of each distribution. Differences in distributions were calculated by two sample Kolomogorv-Smirov tests or one sample test.

Results

Modeling the agent by driving with a series of random forces with a directional bias produced trajectories that were qualitatively similar to those of mosquitoes (Figure 1). We found that the trajectories were qualitatively similar to the behavioral trajectories, except that behavioral trajectories show greater small-scale fluctuation in position.

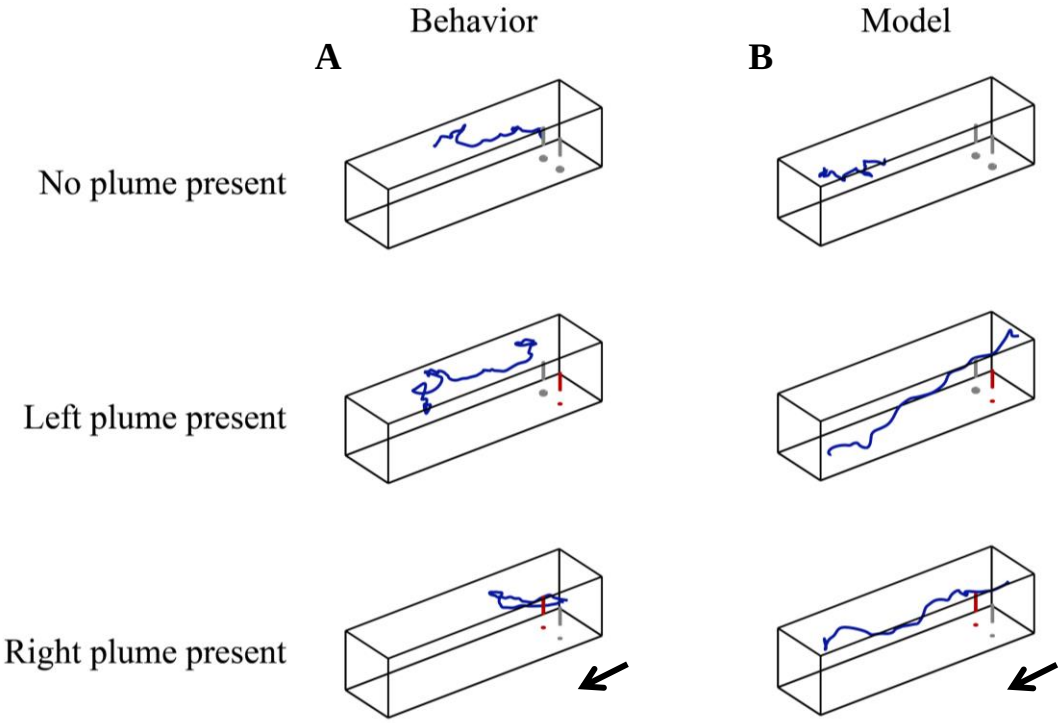

Figure 4.1 – Examples of model and mosquito trajectories. **A**) Example trajectories of mosquito flights. **B**) Example trajectories of agent flights. Positions of heaters are shown with red indicating the element is powered (heated), and grey indicating the element is not. The arrow indicates wind direction.

Optimized model outputs produced average spatial distributions as seen in the behavioral experiments (Figure 2). The upwind distributions produced side biases toward the side of the plume source. The elevation distributions, however, did not capture the pronounced upward bias as observed in the experiments (Figure 2). Similar to behavioral experiments, there is more upwind travel when thermal plumes are present than without.

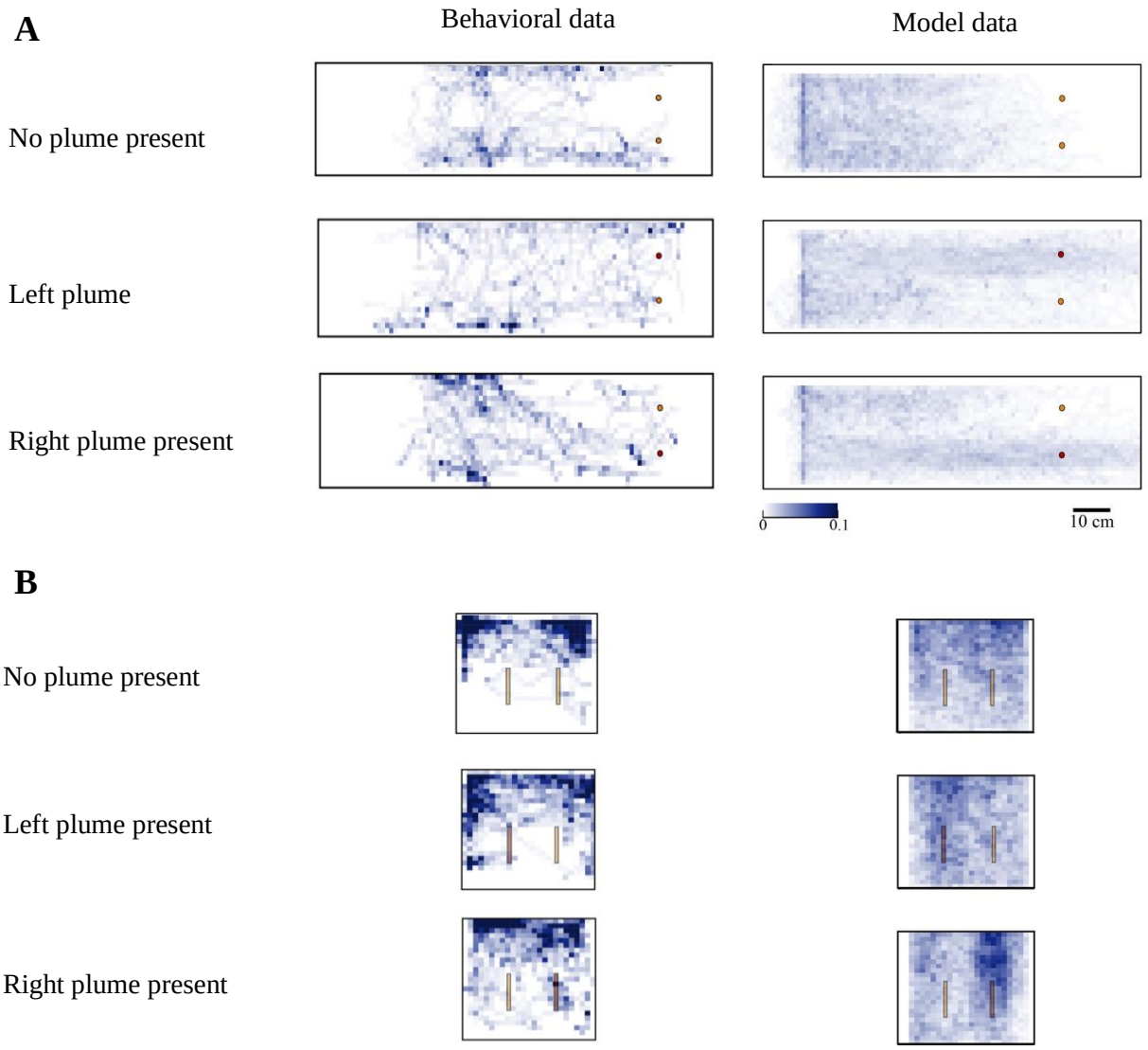

Figure 4.2 – Spatial density of positions. **A**) Plan view and **B**) downwind view of position densities positions with no plume, left plume present and right plume present. Densities from behavioral experiments are shown on the right, model experiments on the left. Darker colors represent higher probability of occurrence. Cylinders are represented as circles or rectangles, respectively. Yellow indicates the heater is off; red indicates heater is on.

Each of the test distributions (left and right plumes present) were found to be significantly different from control and the other test condition in both full and upwind portions of the wind tunnel (Two sample

Kolmogorov-Smirnov, $p < 0.01$, Sign test $p = 1$, Figure 3). This differs from experimental distributions in that the full length distributions not found to be significantly different, and, of the upwind distributions, only the crosswind distributions were significantly different (Chapter III).

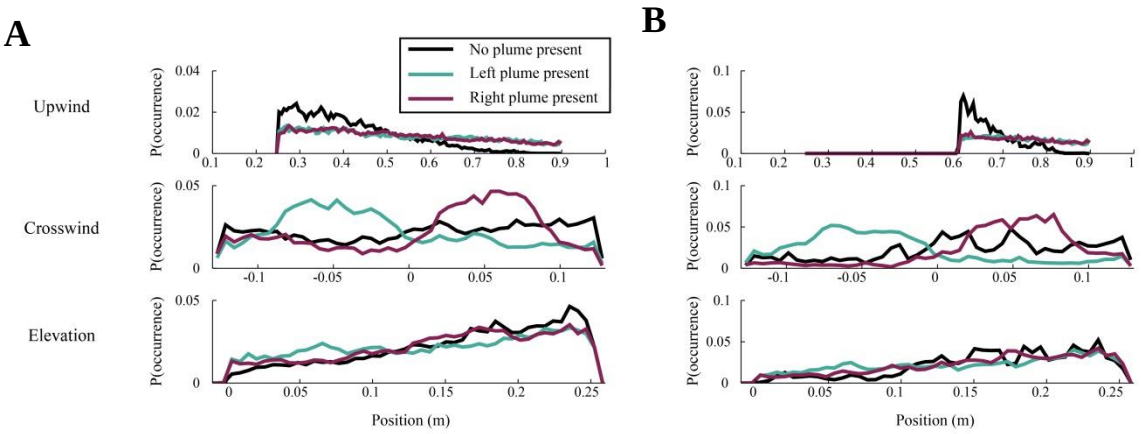

Figure 4.3 – Position distributions of model. Distributions of position in **A**) the full length of the wind tunnel and. **B**) the upwind half of the wind tunnel, for the absence of plume (black), and presence of the left plume (teal) and right plume (purple).

The model output was compared to behavioral data (Figure 4). Overall, the errors between the distributions were quite small, on the orders of 10^{-14} to 10^{-16}. For the control condition, crosswind distributions did not match the behavioral distributions well (SSE > 0.1), however the test conditions (left and right plumes) showed a suitable match (SSE < 0.01).

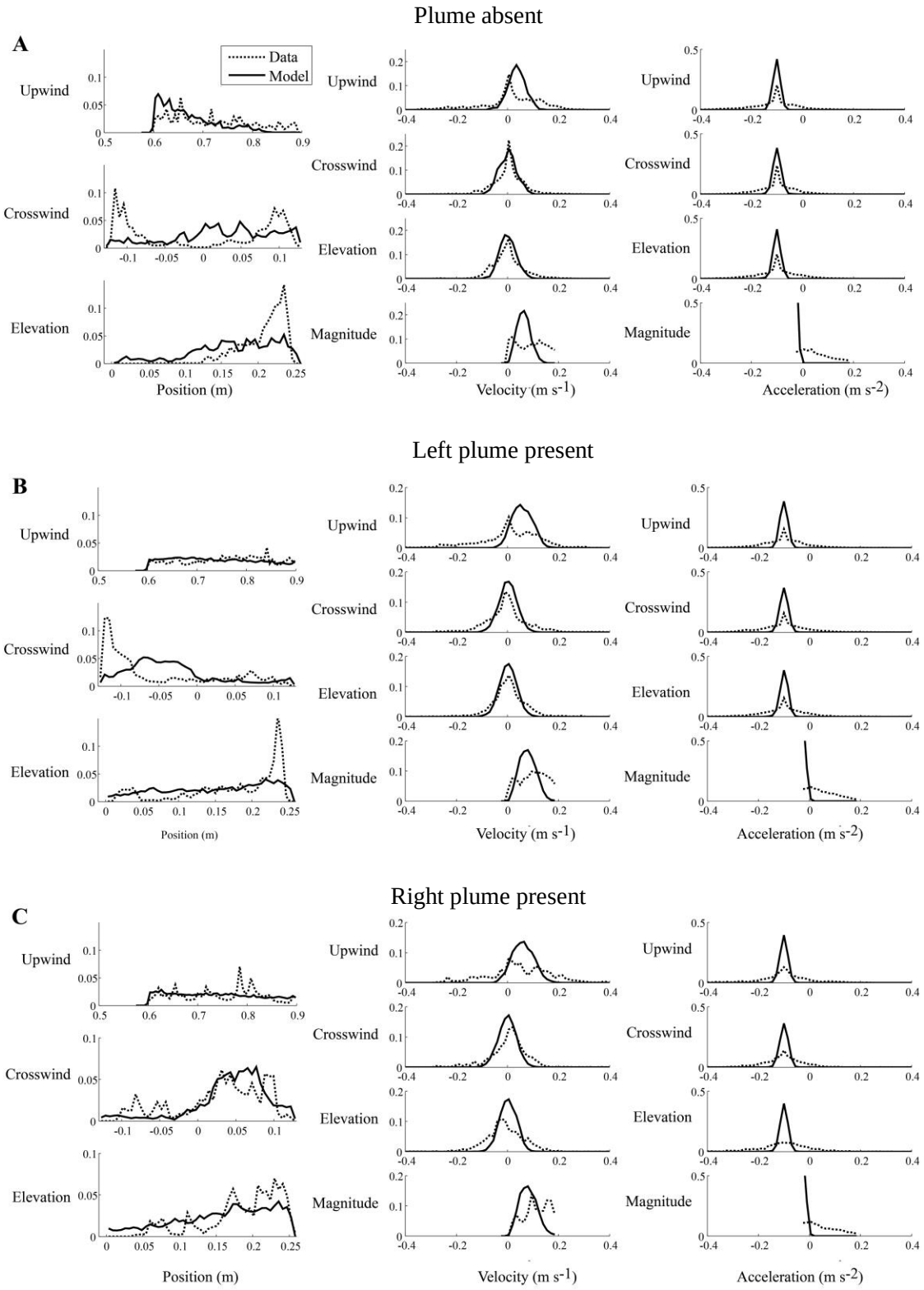

Figure 4.4 – Model performance in comparison to behavior. Comparative distributions of position, velocity and acceleration (left, middle, and right, respectively) for **A**) absent plume, **B**) left plume present, and **C**) right plume present. Dashed lines are the experimental data distributions, while the solid line indicates the model output.

As with the behavioral experiments, we compared behaviors in and out of the plume. For these comparisons, we considered differences across test conditions (no plume, left and right plumes present) and across position (in and out of plume). We found the agents did not spend significantly more time within the plume boundaries than out when the plume was present and absent (two-way ANOVA, $p > 0.05$). The upwind/downwind velocity and acceleration varied significantly by position and presence of the plume. The crosswind velocity and acceleration varied with position of the plume, but not its presence. Unlike with experimental behaviors, vertical (elevation) velocity and acceleration differed significantly with position but not presence.

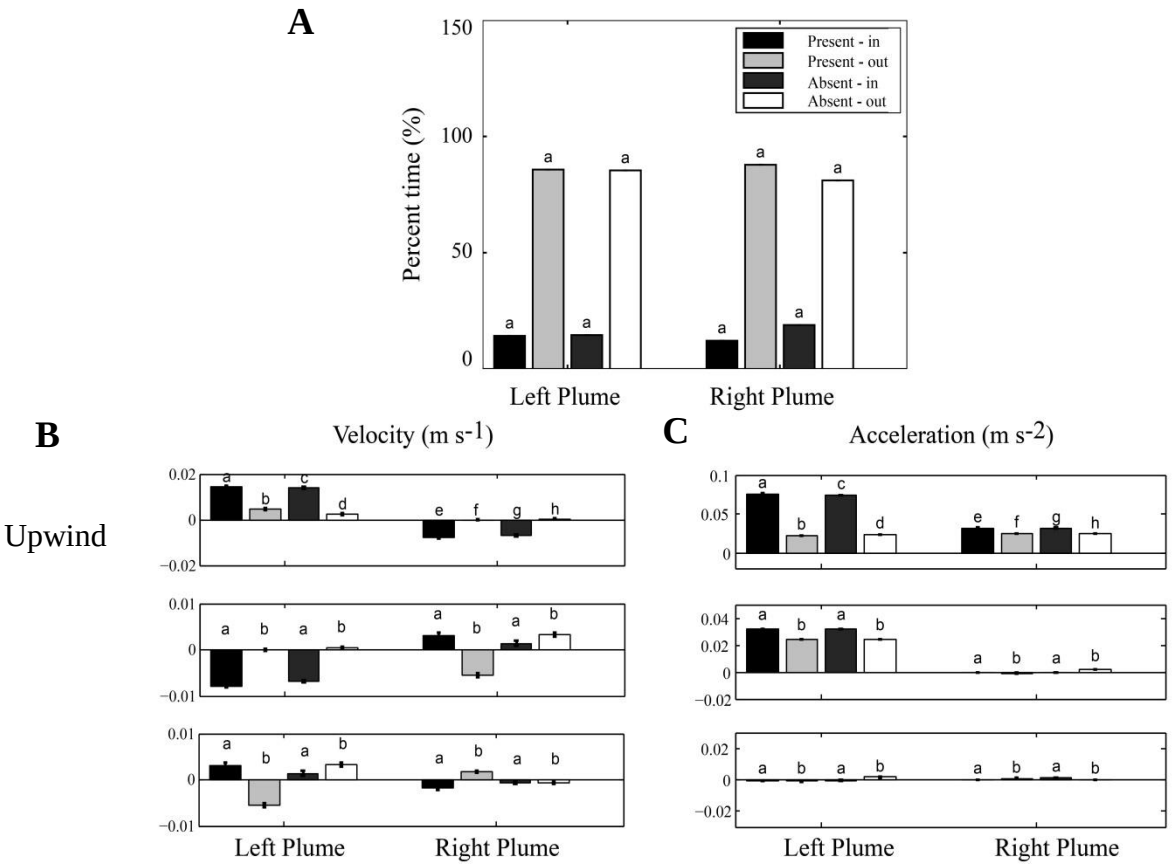

Figure 5 – Model kinematics. **A**) Percent time spent in and out of plume boundaries with plume present and absent, in both positions (left and right) of the plume**. B**) Velocities with plumes present and absent, and in and out of plume position. **C**) Accelerations with plumes present and absent, and in and out of plume position. Vertical plots are upwind, crosswind and elevation. Letters indicate statistical groups; with different letters indicate statistically significant differences across groups.

Discussion

We have presented the primary development of an agent-based model of mosquito plume navigation. We found that we can approximately replicate features of convective thermal plume navigation such as side bias in response to plume presence. In optimizing the weighting of each force involved in the driving force to minimize differences between kinematic distributions, we found there was a tradeoff between goodness of fit such that velocity distributions could be well-fit *or* acceleration distributions could be well-fit. The optimization resulted in distributions that had the similar means and shape, but did not otherwise fit either the velocity distributions or the acceleration distributions (Figure 4).

We were able to produce trajectories that were qualitatively similar to observed mosquito trajectories. However, *en masse*, the agent model flights with the plume absent (baseline) did not match the density or distribution of mosquito trajectories produced when the plume was absent (Figure 1). The main difference observed was the absence of upwind travel in the control (no plume) condition. The mosquito trajectories also had little upwind travel, but the variability of such upwind travel was not seen in the model.

Despite the differences in baseline behavior, we were able to produce position biases in response to the presence of left and right plumes (Figure 2). We observed that the amount of time spent within the plume boundaries was not significantly affected by plume presence. This result is in agreement with the mosquito behavior; however the agent spends slightly more time within the plume bounds than mosquitoes. This result does not indicate, however, that the plume presence has no effects on flight performance. The difficulty of examining mosquito behavior in this experimental paradigm, is the deconvolution of plume effects and the effects of the physical or spatial features of the wind tunnel.

There are three types of outcomes that can occur in the kinematic statistical groups: location dependence, turbulence dependent and plume dependence. Location dependence has statistical groupings dependent on the position of the agent in or out of the plume, but not the presence of the plume. Recall that our two plumes are not equal in temperature and therefor height and diameter (Chapter II Discussion). It could also be that locational dependence in the behavior is the result of difference in signal strength between the two plumes. Turbulence dependence occurs when the statistical groupings depend on the presence of the plumes, but not plume position. This occurrence suggests that the presence of the plume changes the flow of wind or other cues in the environment. Finally, plume dependence occurs when the statistical groupings vary by position and presence of the plume. Findings that fall into this category present two confounds: either the difference in plumes produces a differing response or the sampling of the data is small.

In the upwind trajectory, we found the mean velocity and acceleration varied with both plume position and condition, meaning it was plume dependent (Figure 4.3). This finding is expected, as upwind forces change when the agent is within the plume. We also found, as with behavioral data, that the

crosswind velocity and acceleration are location dependent. We anticipated this finding, as crosswind and elevation forces are affected by the repulsion force. The plume presence also affects crosswind forces, and therefore velocity and acceleration, but since it is not a constant force, the probability of biasing mean kinematics is small. Thus we can assert that, thus far, we are modeling crosswind positional or spatial influences on our agent, possibly in a fashion similar to what we observe in mosquito flight. Further work is required to confirm this effect. If robust, we may be able to elucidate spatial- and plume-related influences on mosquito flight.

Some of the differences seen between the behavioral and model behavior can be attributed to the sample sizes. The agent model statistics were calculated from 200 trajectories, while there were about 40 mosquito trajectories. Further, the behaviors were strictly deterministic. Future work on the model should perhaps include a higher variance across conditions, which can easily be achieved by adding stochasticity to the model, such as probabilistic plume detection, or execution of states.

These results show, for the first time, that mosquito flight is well described by a biased (upwind) random walk, and that flights can be reproduced by manipulating a collection of forces acting on a mass. We were also able to reproduce the large scale, position biases seen in behavioral experiments, although adjustments should still be made to produce the expected kinematics. To our knowledge, this is the first model to characterize plume structure and agent flight in three dimensions.

We have presented here the preliminary formulation of an agent-based model that approximates the kinematics of mosquito flight in a turbulent, convective thermal plume. We were able to capture the side bias seen in behavioral experiments with the plume present, but were not able to replicate baseline positional distributions or some of the kinetic distributions (not shown). The primary focus for further development of the model will focus on the optimization strategy, namely finding a score or optimization approach that is better suited to matching both the velocity and acceleration distributions of the control behavioral data. We could, for example, employ a genetic algorithm.

There is room, also, to reconstruct the formulation of the model. At present, the baseline, or control, behavior seen in mosquitoes is replicated largely using the repulsion force, $F_{repulsion}$. This force is constantly applied, with a position-dependent magnitude. This force serves to encourage the agents into regions of the wind tunnel in which mosquitoes were observed to spend their time. It may be more effective to model this position bias using one or two spring constants. Thus, the forces serve to push the agent throughout the volume, and the tendency toward these regions is governed by the spring constants. Thus Eq 4.1 becomes:

$$F_{total} = -\eta\vec{v} - (k_1 + k_2)\vec{x} + F_{driving}, \tag{4.3}$$

where k_1 and k_2 are spring constants for attraction to preferred regions in the crosswind dimension.

Given the optimization technique, this would require another optimization variable (the spring constant), resulting in a higher dimension, and more computationally taxing search. The exploration of this space through the optimization, however, may result in a better exploration of space and perhaps a better fitting of the kinematic distributions.

Finally, the model, at present does not calculate a behavioral performance measure. Because discrete events, such as landing, occurred to rarely to be compared across conditions, it cannot be used as a reliable end-point for mosquito trajectory. Many mosquitoes spent time hovering around the heating cylinders, so a performance measure derived from agents (and mosquitoes) entering into a target zone may provide a better score for optimization.

Here we have provided the groundwork for a dynamic, agent-based model that not only encompasses behavioral response but also employs some history of detection, making it a cognitive-reactive model. We have shown we can qualitatively reproduce the trajectories of a mosquito in a wind tunnel. The drawback of this model is that the baseline behavior is constrained to that observed in this specific wind tunnel and behavioral setup. To broaden the application of this model, one would have to elucidate the mechanisms driving the positional bias (wall following) seen in the behavioral experiments. Still, one can easily augment this model to reflect their particular experimental set up, including plumes with various statistics. There are many knobs, so to speak, that can be addressed with this model, allowing it to be fine-tuned not only to thermal plume response, but to virtually any windborne sensory stimulus.

References

Bachmayer, R., & Leonard, N. E. (2002, December). Vehicle networks for gradient descent in a sampled environment. In *Decision and Control, 2002, Proceedings of the 41st IEEE Conference on* (Vol. 1, pp. 112-117). IEEE.

Bau J, Cardé R. (2015). Modeling optimal strategies for finding a resource-linked, windborne odor plume: theories, robotics and biomimetic lessons from flying insects. *Integrative and Comparative Biology*. (*In press*).

Belanger JH, Willis MA. (1998). Biologially-inspired search algorithms for locating unseen odor sources. Proceedings of the 1998 IEEE ISIC/CIRA/ISAS Joint Conference.

Brown, A. W. A. (1951). Studies of the responses of the female Aedes mosquito. Part IV. Field experiments on Canadian species. *Bulletin of Entomological Research*, **42**(03.

Dekker T, Cardé R. (2011). Moment-to-moment flight manoeuvres of the female yellow fever mosquito (Aedes aegypti L.) in response to plumes of carbon dioxide and human skin odour. *J Exp Biol*. 214.

Dusenbery D. (1997). Upwind searching for an odor plume is sometimes optimal. *Journal of Chemical Ecology*. 16(6).

Farrell JA, Murlis J, Long X, Li W, Cardé R. (2002). Filament-based atmospheric dispersion model to achieve short time-scale structure of odor plumes. *Environmental Fluid Mechanics*. **2**(1-2).

Geier M, Bosch, O, Jurgen B. (1999). Influence of odour plume structure on upwind flight of mosquitoes towards hosts. *Journal of Experimental Biology*. **202**.

Grunbaum D, Willis MA. (2015). Spatial memory-based behaviors for locating sources of odor plumes. *Movement Ecology*. **3**(1).

Huang C, Hsing T, Cressie N, Ganguly AR, Protopopescu VA, Rao NS. (2010). Bayesian source detection and parameter estimation of a plume model based on sensor network measurements. *Stochastic Models in Business and Industry*. **26**.

Iams, S. M. (2012). Free flight of the mosquito Aedes aegypti. *arXiv preprint arXiv:1205.5260*.

Lochmatter, T., & Martinoli, A. (2009, May). Theoretical analysis of three bio-inspired plume tracking algorithms. In *Robotics and Automation, 2009. ICRA'09. IEEE International Conference on* (pp. 2661-2668). IEEE.

Maekawa E, Aonuma H, Nelson B, Yoshimura A, Tokunaga F, Fukumoto S, Kanuka H. (2011). *Parasites and Vectors*. **4**:10.

Martinez D and Moraud EM. (2013).Reactive and cognitive search strategies for olfactory robots. Neuromorphic Olfaction. CRC Press. Boca Raton, FL.

McMeniman C, Corfas R, Matthews B, Ritchie S, Vosshall L. (2014). Multimodal integration of carbon dioxide and other sensory cues drives mosquito attraction to humans. *Cell*. **156**.

Pang, S., & Farrell, J. (2006). Chemical plume source localization. *Systems, Man, and Cybernetics, Part B: Cybernetics, IEEE Transactions on, 36*(5), 1068-1080.

Vergassola, M., Villermaux, E., & Shraiman, B. I. (2007). 'Infotaxis' as a strategy for searching without gradients. *Nature*, *445*(7126), 406-409.

V.
Concluding Remarks

Here I have shown the female yellow fever mosquito, Aedes aegypti—a vector for many debilitating and deadly diseases—navigates toward the source of convective thermal plumes that are turbulent in nature (Chapter III). This behavior was observed by minimizing the radiative emissivity of a thermal source, providing only robust convective thermal signals (Chapter II). I was able to reproduce the positional bias observed in behavioral experiments using an agent model of mosquito flight. I suggest that this navigation is the result of a slow oscillation (> 50 mHz) of directional bias applied to a flight well-characterized as a random walk (Chapter IV). This slow oscillation may be an optimal form of plume navigation, as optimization of plume navigation in an agent based model has resulted in a similar behavior (Belanger and Willis, 1998, citation referenced in Chapter IV). Features of this oscillation, such as onset, frequency distribution and amplitude, are yet to be determined.

This behavioral finding is important for development of effective, affordable, and most importantly, accessible mosquito traps in disease-laden areas of the world, as manipulation of thermal signal is menially accomplished. Such developments, of course, require further work in behavioral experimentation; specifically focusing on defining statistical features that influence flight, and discrete behavioral responses, if any. There is a confound in the experimental approach outlined here, in that it is unclear whether the flight kinematics and trajectories we observed are in response to turbulent air structure or thermal plume structure. This confound is a common one, often The behavioral model presented in Chapter IV lays the groundwork for developing powerful tools with which one can elucidate this confound. Is the proposed biased random walk observed in convective thermal plume navigation an efficient form of navigation in a turbulent regime, or is it a constraint of the signal salience or flight mechanics of a mosquito?

The application of agent models and behavioral policy of mosquitoes is vast—with potential avenues in prevention of vector-host interaction, as well as robotics and other technological advances. However, the value of such research, I believe, should be in the dissemination of knowledge to those who would benefit from it the most. The big picture aim of eradicating global diseases, such as malaria, is not in the hands of *a* scientist, but *each* scientist. I conclude this research with the assertion that sharing one's work (especially beyond the scientific community) is as valuable as the work itself.